Master Thesis

submitted within the UNIGIS MSc. programme
at the Department of Geoinformatics - Z_GIS
University of Salzburg, Austria
under the provisions of UNIGIS India framework

Assessment of Forest Canopy Cover Change in Parsa National Park, Nepal (1989-2019)

by

Suraj Joshi
U105358

A thesis submitted in partial fulfilment of the requirements of
the degree of
Master of Science (Geographical Information Science & Systems) – MSc (GISc)

Advisor:
Dr. Shahnawaz
University of Salzburg, Austria

Co-advisor:
Dr. Him Lal Shrestha
Kathmandu Forestry College, Nepal

Kathmandu, July 2021

Science Pledge

By my signature below, I certify that my thesis report is entirely the result of my own work. I have cited all sources of information and data I have used in my report and indicated their origin.

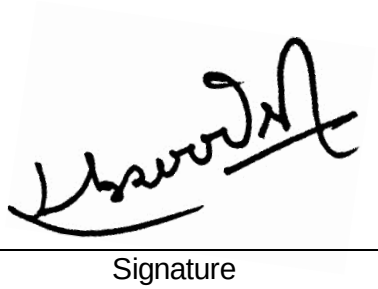

Kathmandu, Nepal July 2021	
Place and Date	Signature

Acknowledgements

First and foremost, I would like to thank my advisor Dr. Shahnawaz for his continuous guidance during my academic project and thesis. His valuable and critical feedbacks helped a lot to bring my work to a higher standard. I would also like to thank my co-advisor Dr. Him Lal Shrestha for his support and encouragement throughout my studies.

Finally, I would like to thank my family and my friends Nishan Baral, Nitant Rai and Rijan Sharma for their continuous moral support.

Abstract

Forests provide a wide variety of goods and services, and most of them are better received when the forests are left undisturbed. In spite of that humans are continuously exerting pressure on the forests. Deforestation is a major concern worldwide, and forest cover changes are often measured in terms of areal change, but besides that, Forest Canopy Cover (FCC) change can is also an important characteristic as it significantly influences the local climate and thus the distribution and health of plant and animal species.

Various studies suggest a positive change in the forest cover in the mid hills of Nepal, but the same is not true for terai region. Studies report that the forests of terai have been modified significantly by humans. Parsa national park lies in Bagmati province and Province 4 in the terai region of Nepal. This park is of great ecological and socio-economic importance. It is reported that most of the forest areas in the park have been restored after its establishment, but still humans are exerting pressure to the forests thus period monitoring of the forest is essential. Furthermore, lack of forest cover change studies in the park makes it urgent. Thus, this study aims to assess the FCC change in Parsa national park from 1989 to 2019. There are many remote sensing approaches to study FCC in an area ranging from simple aerial photo interpretation to more complex methods like LiDAR, Artificial Neural Networks (ANN), Forest Canopy Density (FCD) model and multiple regression. For this study Rikimaru`s (1996) FCD model was selected due to its low cost and time requirement. Also, since the model is based on Landsat images, historical analysis is possible.

FCC change was studied from 1989 to 2019 using Landsat images of 1989, 2003 and 2019. The result shows that even though forest area has not changed much between the study periods, there was considerable change in FCC. In both periods (1989-2003 and

2003-2019), mostly the forest areas with higher FCC i.e., 60.1-100% have changed significantly as compared to lower classes. A positive trend of FCC change was observed in the core zone, whereas the FFC change in the buffer zone was mostly negative from 1989 to 2003 and positive from 2003 to 2019. In contrast to that, the forest in the northeastern part of the buffer zone had positive change in both the time periods indicating a positive trend. In terms of intensity/degree of FCC change i.e., percentage increase/decrease in FCC, majority of the increase and decrease were found to be between 0.1% to 25%. FCC in some parts of the buffer zone were found to be increased by more than 25%, and even by more than 50% from 2003 to 2019. In contrast to that, in the same period, FCC in some parts of the extended park area to the south-east was found to be decreased by more than 25%. A negative trend was observed for the same parts of the extended area.

Table of Contents

Contents

List of Tables

List of Figures

List of Maps

Abbreviations

6S – Second Simulation of Satellite Signal in the Solar Spectrum

ASTER – Advanced Spaceborne Thermal Emission and Reflection Radiometer

ANN – Artificial Neural Networks

AVI – Advanced Vegetation Index

AWEI – Automatic Water Extraction Index

BI – Bare soil Index

DEM – Digital Elevation Model

DFRS – Department of Forest Research and Survey

DN – Digital Number

FAO – Food and Agriculture Organization

Esri – Environmental Systems Research Institute

FCC – Forest Canopy Cover

FCD – Forest Canopy Density

GEE – Google Earth Engine

GIS – Geographic Information System

ha – Hectare

ISODATA – Iterative Self-Organizing Data Analysis Technique

ITTO – International Tropical Timber Organization

JOFCA – Japan Overseas Forestry Consultants Association

L1 TP – Landsat level-1 Terrain and Precision Product

LaSRC – Land Surface Reflectance Code

LEADPS – Landsat Ecosystem Disturbance Adaptive Processing System

NDSI – Normalized Difference Sand Index

NDTI – Normalized Difference Tillage Index

NDVI – Normalized Difference Vegetation Index

OLI – Operational Land Imager

RF – Random Forest

SI – Shadow Index

SSI – Scaled Shadow Index

TM – Thematic Mapper

TOA – Top of Atmosphere

USGS – United States Geological Survey

VD – Vegetation Density

WRS - Worldwide Reference System

Chapter-1: Introduction

1.1. Background

Forests are one of the most important natural resources of our environment as they provide a wide range of goods and services to the living beings. They provide wood for timber and fire, provide medicinal plants, genetic resources and biodiversity, regulate water, temperature and nutrient cycle, absorb carbon dioxide gas, protect soil from erosion and so on. Changes in forest cover affects the delivery of these goods and services, and most of the environmental benefits are best received when forests are left undisturbed (FAO, 1995).

Forest cover change over a period of time is usually described in terms of forest cover loss and gain, or land use land cover conversions associated with forests (Hansen et al., 2013). But besides that, forest also changes in structure and composition due to various natural and anthropogenic drivers that may not change the forest extent. One such type of change which represents structural change in a forest is forest canopy cover (FCC). FCC is the percentage of a forest area covered by vertical projection of the tree crowns (Jennings, 1999). Even though deforestation is the primary concern, but the assessment of FCC is equally important to assess overall forest condition. FCC is an important characteristic of a forest as it influences the sunlight, humidity, temperature and soil moisture, thus affecting the vegetation composition, health and distribution of wildlife (Echeverría et al., 2007; Jain et al., 2020). Since there is no single standard to measure forest health, change in canopy cover is often taken as a proxy to assess the forest health or condition as it is easier to quantify (Jain et al., 2020; Panta et al., 2008; Sahana et al., 2015). Even if a forest area has remained the same between two different dates, the change in its canopy cover can have drastic impact on the environment (Lambin et al., 2003). Thus, along with the deforestation, monitoring FCC is of vital importance and can

provide a deeper insight into the overall forest condition enabling the managers to select the best management practices for a certain forest area.

In the context of Nepal, forest covers 40.36% out of the total area (DFRS, 2015). Besides the environmental benefits, the role of forests is crucial in Nepal`s socio-economic development due to high dependency of the rural population on the forest resources for fuel, fodder, timber and non-timber forest products (Chaudhary et al., 2016); the same is also true for Parsa national park. Centralized forest management approach was practiced in Nepal before the 90s that excluded local people from utilizing the forest resources. This approach was not able to protect the forests from degradation and deforestation because the local people did not have the feeling of ownership and thus did not consider it their responsibility to protect the state-owned forests. In the early 90s, after the introduction of Community Forestry Act, large no. forest areas were handed over to the local people giving them right to manage and utilize the forest resources (Nagendra, 2002; Pathak et al., 2017). Various studies suggest that this approach of decentralized forest management has been successful in restoring the forests, particularly in the mid hills, but its effectiveness in the lowlands or the terai region is still considered debatable. There was mass migration from the hills to terai since 1960 after malaria eradication. This migration has not only increased human pressure on the terai forests, but an increased ethnic diversity and inequality has made the community-based forest management approach difficult to implement in the terai. Studies have reported that human induced deforestation, degradation and fragmentation have significantly modified the terai forests (DFRS, 2014; Nagendra, 2002; Panta et al., 2008; Reddy et al., 2018). According to Reddy et al. (2018), from 1975 to 2014, the overall loss of dense forest was higher as compared to open forest; and the spatial changes in tropical deciduous Sal forests and sub-tropical broadleaved forest was more as compared to other forest types.

Parsa National Park lies in the terai region of Nepal and was initially established as a wildlife reserve in 1984 for the protection of wild Asian elephants and their habitat and covered an area of 499 Km^2. Today the park covers a total area of 624.39 Km^2, out of which 339.19 Km^2 constitutes the core zone of the park which is strictly protected and 285.3 Km^2 the buffer zone. The buffer zone was declared around the park to reduce human pressure on the core zone. Forests in the buffer zone are managed and utilized the by the local people and ecofriendly development activities are allowed inside it to promote overall livelihood development of the local people. Before the establishment of the reserve, the forest was under heavy anthropogenic pressure. It is reported that majority of the forests have been restored after the establishment of the reserve, still, the park suffers from problems like encroachment and illicit felling. Furthermore, population growth around the buffer zone and no clear demarcation of park boundary is making the problems worse (Parsa National Park, 2018). These issues can significantly affect the forest canopy cover if not monitored and controlled in time. Furthermore, ecological sensitivity of the park and no local level previous studies regarding forest canopy cover makes it more important and urgent to understand the spatio-temporal pattern of the FCC change in the park. Thus, this study aims to assess FCC change in Parsa national park from 1989 to 2019. This study will help the forest managers to devise and implement effective forest management strategies to improve the forest condition and ensure sustainable long-term benefits to the local people.

1.2. Study Area

Parsa national park is located in central Nepal covering parts of Province 2 and Bagmati Province. It covers a total area of 627.39 Km^2 and cover parts of Parsa, Bara and Makwanpur district. It is connected with Chitwan national park to the west, Valmiki tiger reserve of India in the south-west and large areas of national forests to the north and east. It has Rapti river as boundary in its north and Tribhuvan highway in the east. The location of the park is shown in the Map 1.

Parsa national park was initially established as a wildlife reserve in 1984 for the protection of wild Asian elephants and their habitat and covered an area of 499 Km^2. Later in 2005, a Buffer Zone covering an area 285.3 Km^2 was declared around the park to allow local people to manage and utilize the forest resources, and to allow development activities inside the park. In 2015, additional area of 128.39 Km^2 of national forest was added to the existing reserve; with this extension, it was given the status of national park in 2017 (Parsa National Park, 2018).

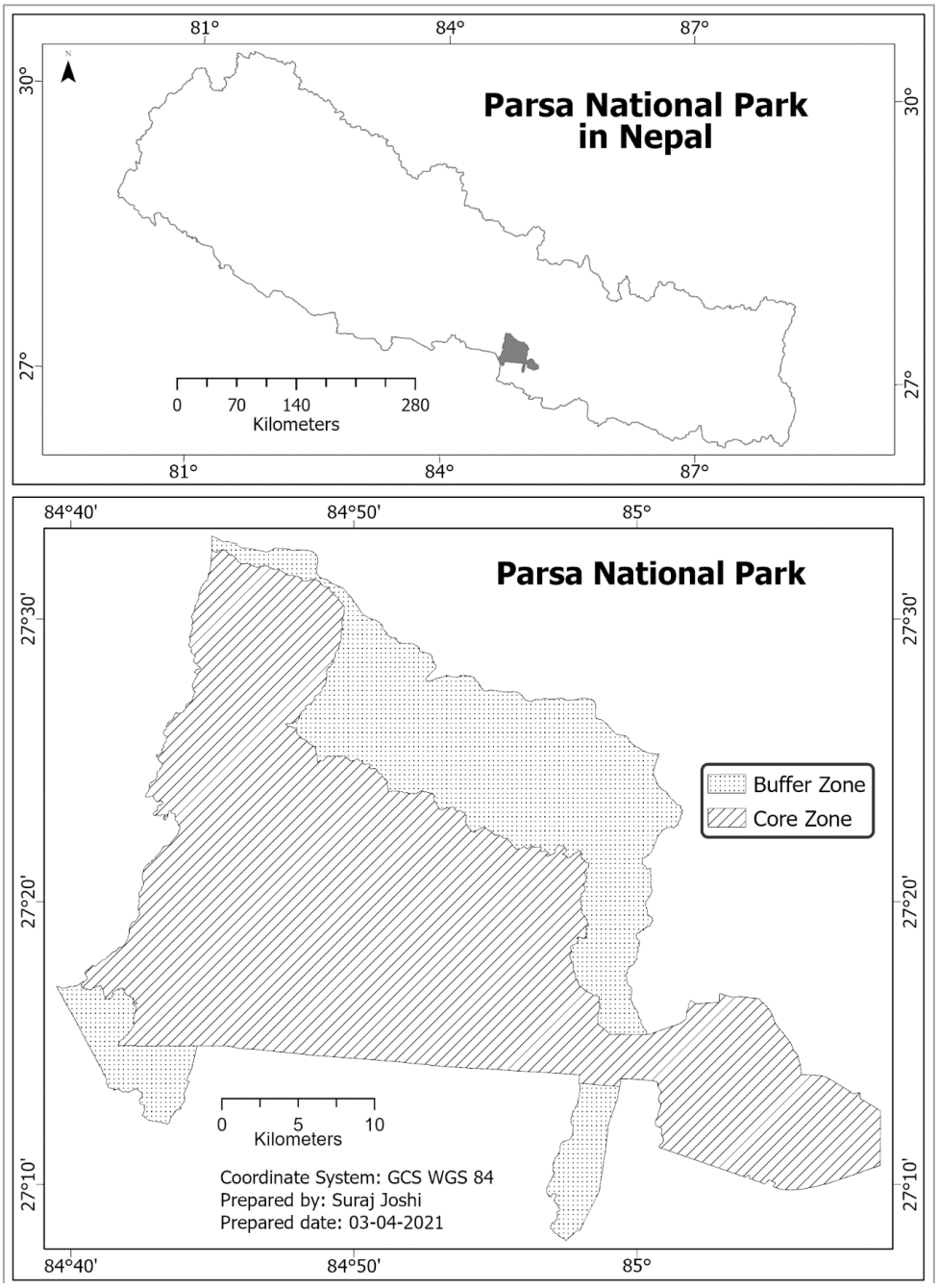

Map 1: Study area

1.2.1. Terrain

The altitude to Parsa national park ranges from 100 to 950 meters above the mean sea level. The park can be divided into three physiographic zones - Churia, Bhawar, and Terai. The Churia and Bhawar zones (lying 250 m above mean sea level) cover about 62.5% of the total area, while terai covers about 37.38%. The terai region is mostly flat, whereas the Churia and Bhawar regions are mostly rugged along with flat agricultural plains and stream banks. There are numerous streams in the area, but most of them are seasonal. All streams disappear in the Bhawar region due to extreme dry and porous soil and resurface in the south outside the park boundary. During monsoon the streams change their course every year and cause flooding in the low-lying areas (Parsa National Park, 2018). The terrain of Parsa national park is represented in Map 2.

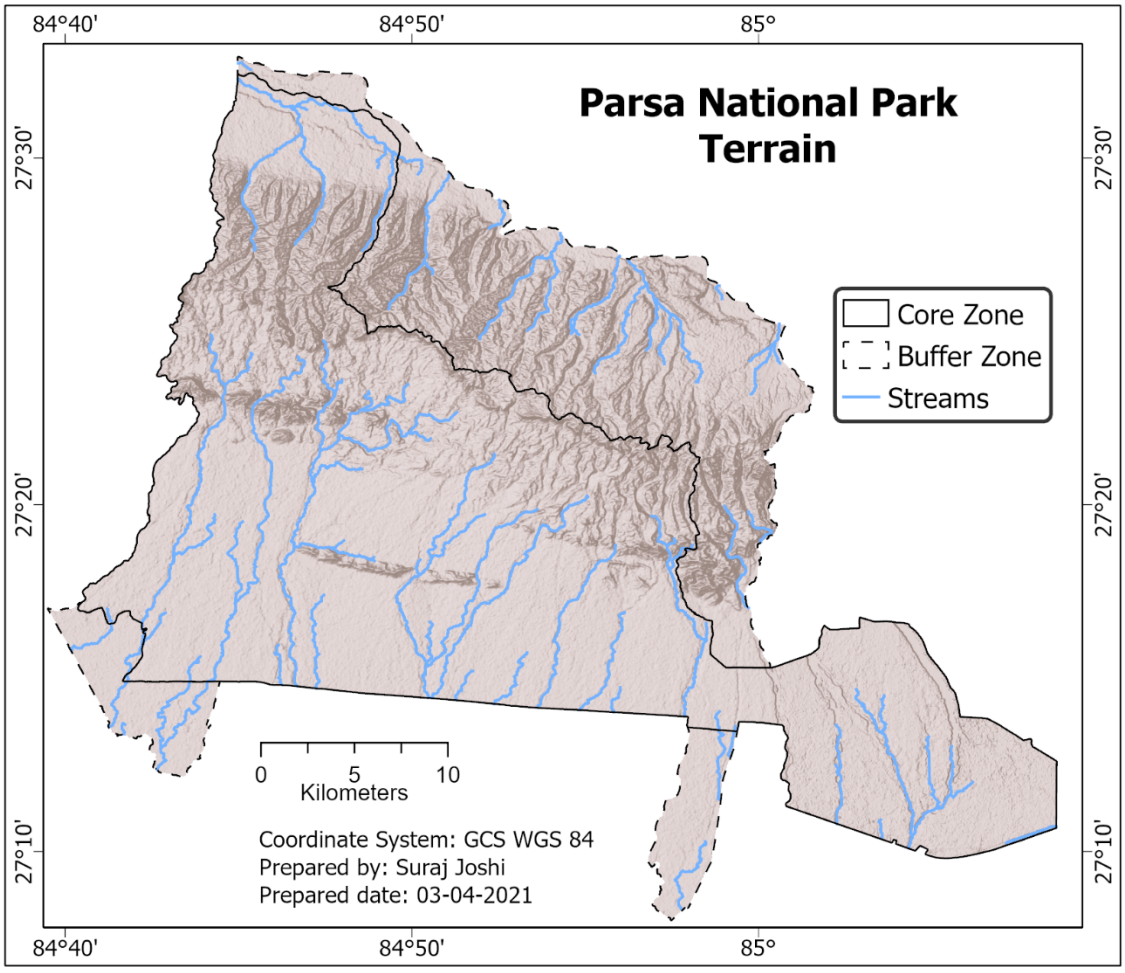

Map 2: Parsa national park terrain

1.2.2. Climate

Parsa national park lies in the sub-tropical climatic zone and experiences four distinct seasons- summer, monsoon, winter and spring. Summers are extremely hot and dry temperature reaching up to 39 °C. It extends from May to July. The monsoon starts from July and ends in September. The average annual rainfall is greater than 1000 mm and the park receives 83% of the total rainfall during monsoon. Winter extends from November to January and is characterized by very cold evenings and mornings temperature reaching up to 7 °C. Spring is characterized by mild temperatures, clearer sky but drier air and land and extends from February to April (Parsa National Park, 2018).

1.2.3. Flora and Fauna

Altogether, 336 species of plants are found in Parsa national park. In terms of forests, it consists of tropical and sub-tropical forests dominated by Sal and its associated species. However, a variation in forest types can be observed according to terrain and local climate in different parts of the park. Major forest types in the parks are mixed deciduous hardwood forest, Sal forest, Sal-Pine forest, Pine forest and Sisoo-Khair Forest.

Altogether, the park harbors 37 species of mammals, 490 species of avian fauna, 13 species of reptile, 3 species of amphibians and 8 species of Pisces. The park is home to some of the protected animal species such as Asian elephant, gaur, royal bengal tiger, striped hyena, one-horned rhinoceros, wild dog, python, giant hornbill, lesser adjutant and sarus crane (Parsa National Park, 2018).

1.2.4. Ecological and Socio-economic Significance

- The national park is representative sample of historical “Char Koshe Jhadi” remaining in the Terai region.
- It is home to many endangered species of animals like Asian elephant, royal bengal tiger, one-horned rhinoceros and gaur.

- The park harbors a large resident population of endangered Asian elephants.
- It is connected to Chitwan national park in the West, Valmiki tiger reserve in the southwest and various other national forests, thus provides an extended habitat and dispersal site to wildlife.
- The forests in park`s buffer zone provides nearly 4893 households with firewood, fodder, timber and other forest products.
- Although the park is visited only by a small no. of tourists each year, it can be developed as a tourist center by promoting eco-friendly and community-based tourism (Parsa National Park, 2018).

1.3. Objectives

The aim of this study is to assess the long term spatio-temporal change in FCC inside Parsa national park from 1989 to 2019 using remote sensing and GIS techniques. The specific objectives to achieve this aim are as follows.

i. Detect the spatial distribution of FCC in Parsa national park in 1989, 2003 and 2019.
ii. Study and document the spatio-temporal change in FCC inside the park from 1989 to 2003 and 2003 to 2019.
iii. Compare FCC change in the core and buffer zone of the park.

1.4. Literature Review

Forest canopy structure constitutes the spatial arrangement of above-ground photosynthetic (leaves) and non-photosynthetic (branches, boles) parts of a forest that have a direct influence on the availability of light. There are two basic measures of forest canopy structure- Forest Canopy Cover (FCC) and Canopy closure/Canopy density. Despite that these two terms represent different aspects of canopy, they are often confused with one another and are found to be interchangeably used in forestry literatures. FCC is the percentage of a forest area covered by vertical projection of the

tree crowns, whereas crown closure is the percentage of the sky hemisphere covered by tree crowns when viewed from a single point (Jennings, 1999; Korhonen et al., 2006; Paletto & Tosi, 2009). The major difference between FCC and crown closure given by Jennings (1999) is illustrated in the Figure 1. As evident from Figure 1, canopy cover estimates represents the proportion of canopy recorded directly above sample points across a sample area, while in canopy closure, the entire sky hemisphere is assessed from a single point with angular measurements (Jennings, 1999).

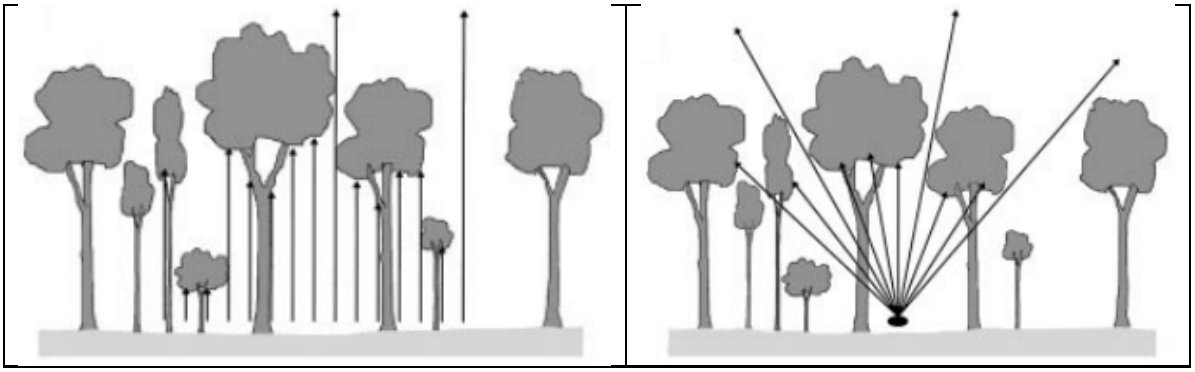

Figure 1: Canopy Cover (Left) Vs Canopy Closure (Right)

FCC is an important stand characteristic as it controls the air humidity and temperature though its influence on the amount and spatial distribution of light, local precipitation and air movement. Thus, it ultimately affects the distribution, growth and health of vegetation and wildlife (Frazer et al., 2001; Henning & Radtke, 2006). Different vegetation and animal species have different requirements in terms local climate, thus manipulation or modification of canopy structure may create favorable environment for a certain species, while at the same time it may adversely affect the growth and survival of others. FCC measurements can be used to study forest growth and health (Jain et al., 2020; Panta et al., 2008; Rikimaru, 1996, Sahana et al., 2015). Thus, monitoring FCC along with the forest conversions can provide a deeper insight about how a forest is changing and help the managers to carryout necessary management interventions to avoid undesirable changes.

In this study, FCC was estimated using a remote sensing based approach called FCD model proposed by Rikimaru (1996). But besides that, there are a number of approaches to measure FCC and can broadly be grouped into field-based approach, remote sensing approach and statistical approach. These approaches are briefly discussed and compared in the following four paragraphs.

Field-based approach involves measuring FCC directly on the study site through sampling. In this approach, FCC samples are taken over a study site using a variety of methods and different instruments. Methods in this approach includes Cajanus tube measurements, line intercept method, spherical and modified Densiometers, hemispherical photographs of canopy and ocular estimation. Research indicates that Cajanus tube, line intercept method, ocular estimation and hemispherical photographs taken with low angle of view are more suitable in measuring FCC, while spherical densiometers and hemispherical photographs taken with wide angle of view are more suitable in measuring canopy closure. Different field-based methods are found to produce variable estimates of FCC. Generally, labor intensive methods like measurements using Cajanus tubes and line intercept methods are more precise and produce less biased results than other aforementioned methods (Korhonen et al., 2006; Paletto & Tosi, 2009).

Statistical approach involves modelling FCC as a function of different forest stand characteristics or variables using regression. In this approach, characteristics or variables that are strongly related to FCC are used to predict FCC values. These variables can be obtained from both field and/or remotely sensed data. Such variables are often readily available from past surveys and include forest stand parameters like basal area, no. of stems and diameter at breast height (Korhonen et al., 2006). In case of remotely sensed data, it may include different bands of satellite images, various spectral indices (e.g., NDVI, band ratios, SAVI etc.) and band transformation products obtained from Principal Component Analysis (PCA) or Tasseled-cap transformation (Carreiras et al., 2006).

Remote sensing approach involves using satellite images, LiDAR data or aerial photos to estimate FCC. They often require data from field-based methods to assess the accuracy of the final results. In remote sensing, there are a wide variety of methods like image classification (Panta et al., 2008), multiple and simple regression, methods involving high resolution satellite images and manual methods like dot-grid method using high resolution aerial imagery (Carreiras et al., 2006), bio-physical modelling (Rikimaru et al., 2002), methods using LiDAR point clouds and LiDAR based Canopy Height Models (Ma et al., 2017). Literatures related to some of the remote sensing methods are discussed in detail in the further sections of this chapter.

In general, compared to the statistical and remote sensing approach, field-based methods like measurement using Cajanus tube and line-intercept provide true FCC estimates, thus are more reliable. But the major drawbacks of these methods are that they are very laborious, time consuming and costly. In addition to that, they don't provide wall-to-wall results making them impractical, particularly in case of large study sites. In contrast to that, remote sensing methods provide much more time and cost-effective means to measure FCC over a large area. Furthermore, the spatio-temporal coverage and resolution of available satellite images enable researchers to study FCC in different time periods and spatial scale. Some important literatures related to FCC estimation using remote sensing are discussed in detail in the following paragraphs.

Carreiras et al. (2006) estimated FCC in montado region of southern Portugal in 1995. Estimation was done using regression models derived using observed canopy cover from high resolution aerial photo and reflectance from various bands and indices derived from Landsat TM image. The study area was dominated by farmlands with oak trees with highly variable tree cover. Their methodology can be summarized into three main steps- (i) canopy cover samples estimation from aerial photos using dot-grid method, (ii) calculation of various indices from the satellite image, (iii) estimation of canopy cover through

regression between the samples and the indices, and samples and Landsat TM bands. A total of 142 canopy cover samples from the study area were collected using an aerial image of 1995. They derived several indices namely NDVI, Soil Adjusted Vegetation Index (SAVI), Modified Soil Adjusted Vegetation Index (MSAVI), Green NDVI (GNDVI), Atmospherically Resistant Vegetation Index (ARVI), VI5, VI7 using the satellite image. Beside these indices, three components of the tasseled cap transformation were also derived. The first component was related to the difference in soil properties, second component was related to the canopy cover, leaf area index and live biomass and the third component was sensitive to the soil and vegetation wetness. Out of the 142 samples, 106 were used for model fitting and 36 for validation. They developed several simple linear and multiple regression models to predict canopy cover over the study. The models were then evaluated using coefficient of determinant (r^2) and adjusted r^2. Model validation was performed using the observed canopy cover values i.e., sample subset of 36 samples and the predicted canopy cover values with the help of various statistical tests.

They reported that the model based on the bands 3, 4, 5 and 7 performed the best with an r^2 of 0.74. Besides that, models based on NDVI (r^2 = 0.72), tasseled cap components (r^2 = 0.70) and ARVI (r^2 = 0.69) also performed well in comparison to others. They found that the presence of undergrowth with different canopy cover can significantly affect a model`s robustness in predicting FCC through satellite images. They concluded that the use of high and medium resolution satellite images could be of vital importance in monitoring canopy cover in areas with highly variable canopy cover.

Ma et al. (2017) evaluated FCC estimates derived from LiDAR data using various LiDAR based equations in Tahae national forest, USA. Their study site was dominated mixed coniferous tree species with shrubs and grasslands. The LiDAR point cloud was obtained in 2012 at a flying height of 600-800 meters. A total of four discrete returns for each pulse was recorded with an average point cloud density of 10 points per meter square over the study area. Before the FCC calculation, they classified the point cloud into ground and

non-ground classes. They also derived a Digital Elevation Model (DEM) and a Digital Surface Model at 1 m resolution using the first returns. They used both point-based and Canopy Height Model (CHM) based approaches to estimate FCC in the study area. In the point-based approach two methods- All Returns Cover Index (ARCI) and First Returns Cover Index (FRCI) were used to estimate FCC. In ARCI, all LiDAR returns beyond a certain height threshold above the ground that intersected with the forest canopy were used in FCC estimation. On the other hand, in FRCI, only the first and single returns were used in the FCC estimation assuming that additional information provided by all the other returns was negligible. Following equations were used to derive FCC using the ARCI and FRCI.

$$ARCI = \frac{\sum All_{canopy}}{\sum All_{total}}$$

$$FRCI = \frac{\sum First_{canopy} + \sum Single_{canopy}}{\sum First_{total} + \sum Single_{total}}$$

Where, All means all returns, First means first returns and Single means single returns. The subscripts total means total number of returns and canopy means the number of returns intersecting the canopy cover i.e., the returns above a certain height threshold.

In CHM based FCC estimation method, first they derived a CHM by subtracting DEM from DSM, then the FCC was calculated as the percentage of pixels with CHM value higher than 2 m within a grid of 30m X 30m.

$$CHM\ Canopy\ Cover = \frac{\sum CHM_{canopy}}{\sum CHM_{total}}$$

Where, CHM_{canopy} means the CHM pixels belonging to the canopy cover i.e., CHM values above 2 meters. CHM_{total} means the total no. of CHM pixels.

They compared the LiDAR derived FCC with field data but observed no strong correlation. They reported that this could be attributed to the limitations of quick field survey method and difference in the level of detail obtained from both the methods. They observed that, as compared to ARCI and CHM method, FRCI method was more appropriate. Furthermore, they reported that a point cloud density of 1 point per meter square was

sufficient for FCC estimation, and the increase in the density has negligible affect on the FCC estimation. They found that the scan angle above 12° from the nadir can induce considerable error in FCC estimates.

Panta et al. (2008) studied the trend of deforestation and degradation in Chitwan national park, Nepal between 1976 and 2001 using Landsat 5 TM and Landsat 7 ETM+ images of 1976, 1989 and 2003. They used image classification using maximum likelihood classifier and post-classification overlay operation to study forest cover change and ANN to predict FCC in the park for 2001. The FCC prediction was done using the reflectance values from Landsat ETM+ bands and training samples collected from field survey. The training samples were collected from 329 training areas in 2002, 2004 and 2006. Out of the total samples, 165 samples were used to predict FCC using ANN and the remaining were used for accuracy assessment. They classified the FCC into four classes- 1-20%, 21-40%, 41-60% and 61-100%. The overall accuracy was estimated to be 82%. Producer`s accuracy between 67% and 77% was observed for the 1-20% and 21-40% classes, whereas accuracy of 98% was observed of the 60-100% class. They have reported that most of the error in FCC prediction was due to misclassification between the non-forest class and 40-60% class. They concluded that deforestation and degradation was mostly observed in forest area with Sal (trees with high timber value), accessible forest areas (forests in flat terrain and near settlements) and forests near the streams.

This study is based on a widely used remote sensing approach to estimate FCC called Forest Canopy Density Mapping model, popularly known as FCD model. It was developed by Rikimaru (1996) as a part of ITTO`s Project PD 32/93 Rev2 (F), “Rehabilitation of Logged-over Forest in Asia-Pacific Region, Sub Project III”. The purpose of the model was to assess the forest condition or growth over a large area in terms of canopy cover percentage to identify the areas which may require rehabilitation treatment, and furthermore help the managers to speculate the intensity of rehabilitation required. It was

developed in order to reduce the cost and time associated with supervised image classification and statistical methods that involve collecting a large number of training samples and require considerable remote sensing skills. FCD model is based on modelling the spectral reflectance of forests to estimate percentage canopy cover through integration of vegetation index, bare soil index, shadow index and thermal index. The methodology was initially tested in South Andaman-India, West Kalimantan-Indonesia, Mindoro Palawan-Philippines and Eastern Forest-Thailand. The initial test results showed that the model was able to produce good results in considerably less time and resources (Rikimaru, 1996; Rikimaru et al., 2002). Figure 2 illustrates how the FCC is assessed by the FCD model as given by Rikimaru (1996).

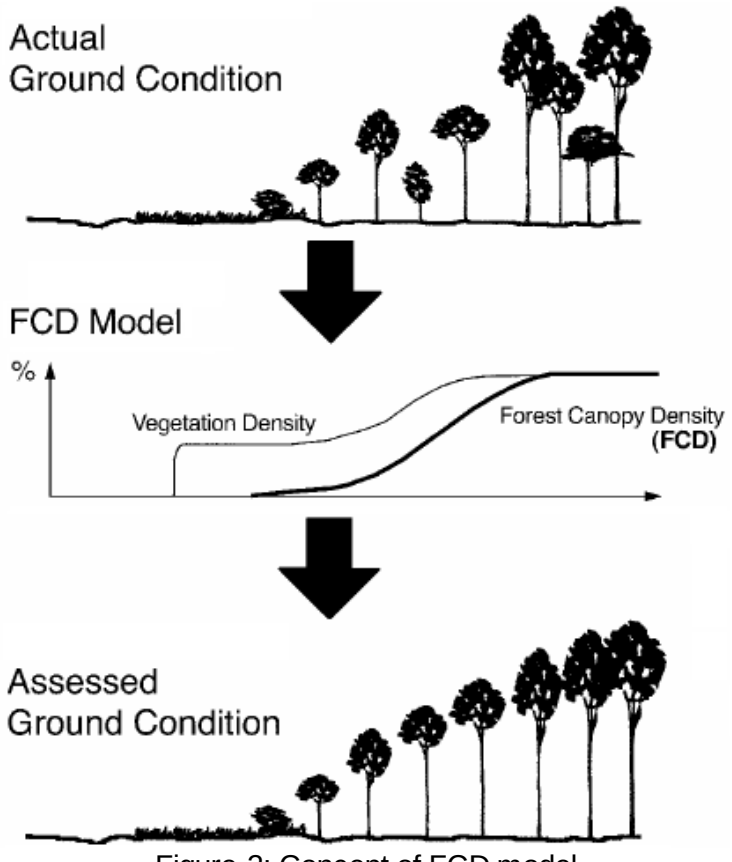

Figure 2: Concept of FCD model

Godinho et al. (2014) demonstrated the effectiveness of FCD model in mapping FCC over mentado region in Portugal with complex argo-silvo-pastoral system. The area was dominated by farmlands with highly variable tree density. After range normalization of bands 1-5 into 0-255 range, they used AVI, BI, SI and TI to estimate the FCC using the

FCD model. Following equations were used to derive the indices using the Landsat TM image of 2003.

$$AVI = \sqrt[3]{[(B4+1) \times (256 - B3) \times (B4 - B3)]}$$

$$BI = \frac{(B5 + B3) - (B4 + B1)}{(B5 + B3) + (B4 + B1)} \times 100 + 100$$

$$SI = \sqrt[3]{(256 - B1) \times (256 - B2) \times (256 - B3)}$$

TI is the ground surface temperature produced using the thermal band i.e., band 6 of Landsat 5 TM. The digital number of Band 6 was first converted into radiance using the coefficients from image metadata, then converted to ground surface temperature i.e., TI using the following equations.

$$L_b = L_{min} + (L_{max} - L_{min}) \times \frac{DN_6}{255}$$

$$TI = \frac{K2}{Ln\left(\frac{K1}{L_b} + 1\right)}$$

Where, L_{min} and L_{max} are the minimum and maximum thermal radiation energies. For Landsat 5 TM L_{min}= 1.238 W/(m^2 steradian) and L_{max}= 15.600 W/(m^2 steradian). DN is digital number of band 6. TI is the effective at-satellite temperature in Kelvin, $K1$= 607.76 W/(m^2 steradian micrometer) and $K2$=1260.56 K.

After obtaining all the indices, they integrated AVI and BI using PCA to produce Vegetation Density (VD) which was then rescaled from 0% to 100%. Since temperature of bare soil and other small vegetation is higher than that of forest, TI was use do differentiate between them. Furthermore, it was used to detect black soil. Black soil has higher temperature and higher SI values, whereas forest has lower temperature and higher SI values, thus TI and SI were used to identify the black soil pixels. Finally, they rescaled the SI from 0% to 100% over the forest area only to obtain Scaled Shadow Index (SSI). They integrated the VD and SSI to calculate FCC using the following equation.

$$FCC = \sqrt{VD \times SSI + 1} - 1$$

They stratified the final FCC into four classes- 0-10%, 11-40%, 41-70%, 71-100% and obtained an overall accuracy of 78% and Kappa coefficient of 0.71. They reported that the accuracy of the FCC estimates increased from lower to higher classes. According to them lower accuracy in lower classes may be attributed to the highly variable tree density in the area coupled with the amount of undergrowth and exposed soil. They concluded that FCD model is an effective way to predict FCC estimates using Landsat images and provide valuable information on the canopy structure at local and regional scales even in the areas having highly variable canopy cover.

Joshi et al. (2006) compared the performance of ANN, maximum likelihood classifier (MLC), multiple linear regression (MLR) and FCD model for estimating FCC using Landsat 7 ETM+ image of October 2001. Their study area was a portion of Sal dominated deciduous forest in Chitwan national park. They assessed the performance of these methods using FCC data collected in field using densiometer and hemispherical photographs in February to March and September to October of 2003. They stratified the FCC into ten classes at equal interval from 0 to 100% and compared the results using Kappa statistics. They also tested their performance using regression between the observed and predicted values through coefficient of determination (r^2), slope and intercept. They observed an overall accuracy of 59.1% (Kappa coefficient= 0.51), 34.4% (Kappa coefficient= 0.23), 49.5% (Kappa coefficient= 0.39) and 44.3% (Kappa coefficient= 0.34) for ANN, MLR, FCD model and MLR respectively. They compared the results produced by the methods using z-tests and found that the results produced by ANN and MLR, and ANN and MLC were significantly different from each other. Similarly result from FCD model and MLR were also found to be significantly different. In contrast to that, the results obtained from ANN and FCD model were found to be similar. They reported that MLA and MLR methods were not able to produce satisfactory results. ANN produced the best result and explained a higher proportion of the variance, but the disadvantage of

using it is that it requires a large dataset for training thus costs more and requires more time. Furthermore, ANN is complicated to use as compared to other methods. FCD on the other hand was found to produce result similar to ANN but the method was found to be prone to biasness and subjectivity from the user while thresholding indices value for separating vegetation, bare soil and forest. They recommend the use of ANN for FCC classification if sufficient resources (time, money and skill) are available, if not they recommended the use of FCD model as it is simpler to use, far more cost and time efficient, and produces similar results to ANN.

The FCD model was selected over other aforementioned approaches for this study because of its simplicity and ability to estimate FCC with considerable accuracy over a large area without significant cost and time. The LiDAR methods are found to produce very good results but are associated with huge costs. In addition to that, in Nepal, LiDAR surveys are not very frequent and have not been done for most of the part of the country in different time periods. This makes FCC change detection using LiDAR impossible. On the other hand, FCD model is based on the use of Landsat satellite images; this not only makes the long-term change detection possible due to availability of Landsat historical images, but also makes it possible to study FCC changes in future since the images are provided to the general public free of cost. Along with the advantages of the FCD model, there are many disadvantages which may reduce the accuracy of the model. The model was made simple enough so that foresters without much knowledge about remote sensing could use it to estimate FCC for large forest areas. In the model, while calculating VD and SSI, thresholding of spectral indices was performed in order to separate vegetation, bare land and forest areas, thus accuracy of the model depended upon selection of proper thresholds. This limitation means that the user most have very good knowledge about the land cover of their study area. This makes the model highly subjective and susceptible to bias. Thus, to deal with this limitation, supervised image classification was performed for all the satellite images to classify the pixels into different land cover classes prior to the

FCC estimation workflow. This will not only decrease the subjectivity but will also reduce the extra burden of separating black soil and forest gaps.

Chapter Summary

Forests provide a wide variety of goods and services, and most of them are better received when the forests are left undisturbed. Forest cover changes are often measured in terms of areal change. Besides that, understanding the FCC change can be of great value as it significantly influences distribution and health of plant and animal species, thus helping us to plan strategies for its management. Various studies suggest a positive change in the forest cover in the mid hills of Nepal but the same is not true for terai region. Studies show that the forests of terai have been modified significantly by humans.

Parsa national park lies in Bagmati province and Province 4 in the terai region of Nepal. This park is of great ecological and socio-economic importance. It is reported that most of the forest areas in the park have been restored after its establishment, but still humans are exerting pressure to the forests thus period monitoring of the forest is essential. Furthermore, lack of forest cover change studies in the park makes it urgent. Thus, this study aims to assess the FCC change in Parsa national park from 1989 to 2019.

There are many approaches to study FCC, among them the remote sensing approach is most widely used due to its low cost, low time requirement and availability of historical data. Remote sensing approach include a no. of methods that can be used to estimate FCC such as LiDAR methods, aerial photos, image classification, linear regression, FCD model etc. The LiDAR and image classification using ANNs are reported to be more accurate methods among them. Due to unavailability of LiDAR data and requirement of huge training dataset for the ANNs, FCD model was selected for this study.

Chapter-2: Methodology

FCC change in Parsa national park was studied using multi-date Landsat images of 1989, 2003 and 2019. Vegetation index, bare soil index and shadow index were integrated to produce the FCC maps for each year using the FCD model. For better identification of land cover classes supervised image classification was performed in Google Earth Engine, and the integration process was carried out in ArcGIS Pro. An overview of the workflow is given in Figure 3, and details regarding the methodology are given in the following sub-headings.

2.1. Used Datasets

The park boundary shapefile created by UNEP and IUCN was used in the study. The shapefile did not have the extended part of the park thus the extended part was digitized from a digital map created by Department of National Parks and Conservation area, Nepal. The digital map was first georeferenced using control points obtained from the grid intersections on the map, then the extended part was digitized in ArcGIS Pro. Later both the datasets were merged to obtain the complete national park boundary.

Table 1: Used Bands of Landsat 5 and Landsat 8 Images

Used Bands	Band no. and wavelength (micrometers) in Landsat 5	Band no. and wavelength (micrometers) in Landsat 8	Spatial Resolution (m)
Blue	B1 (0.45-0.52)	B2 (0.45-0.51)	30
Green	B2 (0.52–0.60)	B3 (0.53 – 0.59)	30
Red	B3 (0.63-0.69)	B4 (0.64-0.67)	30
NIR	B4 (0.76-0.90)	B5 (0.85-0.88)	30
SWIR1	B5 (1.55-1.75)	B6 (1.57-1.65)	30
SWIR2	B7 (2.08-2.35)	B7 (2.11-2.29)	30

Landsat 5 and Landsat 8 image collections from GEE database were used in the study. The forest of Parsa national park is dominated by Sal species. Sal`s leaf fall usually starts from February and completes by the end of April, also, cloud-free images could not be obtained for other months, so images of December were selected for the study. Due to presence of haze in the south-eastern part of the study area in 2003 image, two Landsat 5

images were used in the analysis for that year. Other details regarding the datasets used in this study is given in Table 1 and Table 2.

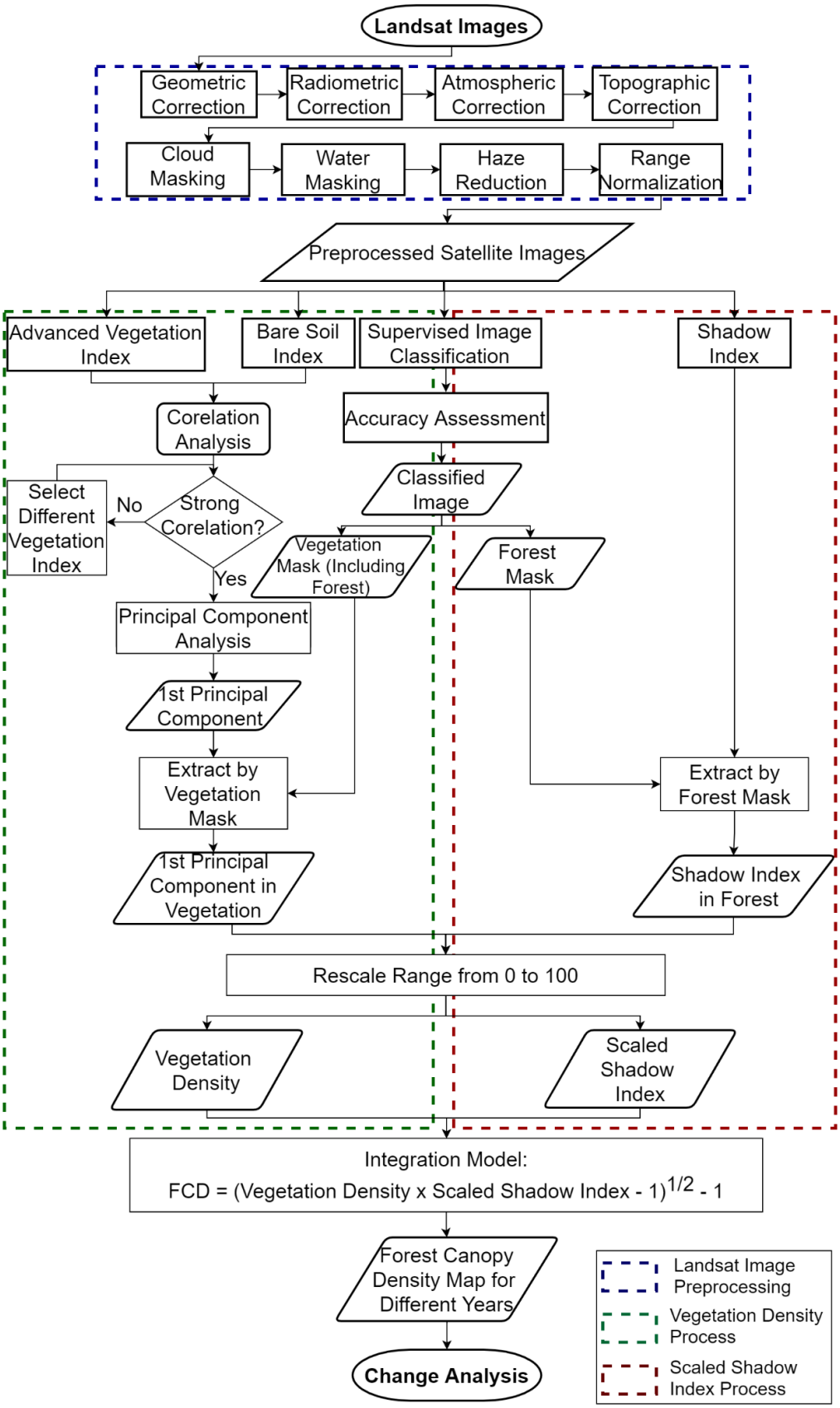

Figure 3: Workflow

Table 2 : Used Datasets

Park Boundary	Source: The World Database on Protected Areas and Department of National Parks and Wildlife Conservation Data Type: Vector
Landsat 5 Images	Source: United States Geological Survey Data Type: Raster Spatial Resolution: 30 meters Date: 1989-12-02, 2003-12-09, 2003-12-25 WRS Path: 141, WRS Row:41
Landsat 8 Image	Source: United States Geological Survey Data Type: Raster Spatial Resolution: 30 meters Date: 2019-12-05 WRS Path: 141, WRS Row:41

2.2. Software

In this study, Google Earth Engine (GEE) and AcrGIS Pro were used during the image processing and analysis. ArcGIS Pro is the latest propriety GIS software developed by Esri, whereas GEE is free-to-use and relatively new GIS platform by Google. ArcGIS is a computer software with user-friendly graphical user interface and ready-to-use powerful tools. This makes ArcGIS Pro an easy-to-use GIS software but resource intensive. In contrast to that, GEE is cloud-based GIS platform; therefore, it is light on user`s computing resources but not as user-friendly as ArcGIS pro. GEE users can use either JavaScript or Python client libraries to perform geospatial procedures. These procedures can be saved and reused, and even shared with other users. In contrast to common GIS software, GEE not only provides geospatial analysis capabilities using JavaScript/Python client libraries but also stores a huge number of ready-to-use datasets. This makes GEE a powerful platform to mine huge collection of datasets and analyze them at the same place, even without powerful computers (Gorelick et al., 2017). Besides GEE and ArcGIS Pro, Microsoft Excel was also used to perform various calculations, and for making charts and tables.

2.3. Image Processing

2.3.1. Image Pre-processing

Various pre-processing procedures must be done before further processing and analysis of satellite images to enhance their quality and to bring them to a desired output. Image pre-processing involves a series of steps to minimize distortions and errors due to sensor, solar, atmospheric, and topographic effects on the imagery. Some of these steps convert the imagery into different units such as at-sensor radiance and top-of-atmosphere reflectance, while others specifically address potential errors such as topographic correction and geometric correction (Young et al., 2017).

This study uses images from different dates, two different sensors, and further requires integration of different spectral indices, thus pre-processing procedures were performed in order to normalize conditions across time, space and sensors and make images more comparable. Pre-processing procedures described below are taken from Young et al. (2017) and Bruce and Hilbert (2006) unless specified otherwise.

i. Geometric Correction

It reduces the errors in relative positioning of the images caused due to variation in altitude, attitude and velocity of the sensor platform, Earth curvature, panoramic distortion, relief displacement and non-linearities in the sweep of a sensor and includes georeferencing and orthorectification. Georeferencing helps to align the images to their correct geographical location and orthorectification address the effects of relief and view direction on the pixels. Geometric correction utilizes ground control points and Digital Elevation Models (DEM). When multiple images are being used for comparison such as in a change detection or for mosaicking or compositing, the alignment of the features in the images should be checked at-least visually and corrected if necessary, otherwise the results from the analysis might be erroneous. The images used in this study were already geometrically corrected by USGS, thus it was not performed.

ii. Radiometric Correction

It accounts for the errors that effect the reflectance value of the pixels caused due to sensor, solar, atmospheric, and topographic effects. Following steps are involved in this correction procedure.

- Conversion to Radiance: Initially the images are in Digital Numbers (DNs), while DNs can be used for single image analysis, they cannot be used to compare images across time due to sensor degradation and sensor differences. Thus, they should be converted to radiance i.e., a comparable scale. DNs can be converted to radiance using the following formula. This formula uses rescaling factors associated with each band which is provided in the metadata file of the Landsat image.

$$L_\lambda = ML \times Q_{cal} + A_L$$

Where,

L_λ = Spectral radiance in Watts/(m^2 * steradian * μm)

ML = Radiance multiplicative scaling factor for the band

A_L = Radiance additive scaling factor for the band

Q_{cal} = Pixel value in DN

This procedure had been already done for the used images by USGS, thus it was not performed during the preprocessing.

- Solar Correction: This accounts for the influence of sun on the pixel values and converts radiance to Top-of-Atmosphere (TOA) reflectance. TOA is a measure of the proportion of incoming radiation reflected from a surface as detected from above the atmosphere. The radiance can be converted to TOA using the following formula. The formula uses the solar irradiance, Earth-Sun distance, and solar elevation angle. These values can also be obtained from the metadata files.

$$\rho\lambda` = M_\rho \times Q_{cal} + A_\rho$$

Where,

$\rho\lambda`$ = TOA Planetary Spectral Reflectance

M_ρ = Reflectance multiplicative scaling factor for the band

A_ρ = Reflectance additive scaling factor for the band

Q_{cal} = Pixel value in DN

The $\rho\lambda`$ derived from the above equation is not true TOA reflectance because it does not contain correction for the solar elevation angle. The users can use the scene-center solar elevation angle in the metadata or calculate their own per-pixel solar elevation angle across the entire scene. Using the solar elevation angle the true TOA reflectance can be calculated as follows.

$$\rho_\lambda = \frac{\rho\lambda`}{\cos(\theta_{SZ})} = \frac{\rho\lambda`}{\sin(\theta_{SE})}$$

where:

ρ_λ = TOA planetary reflectance

θ_{SE} = The scene center sun elevation angle

θ_{SZ} = Local solar zenith angle; $\theta_{SZ} = 90° - \theta_{SE}$

(USGS, 2019)

This procedure had been already done for the used images by USGS, thus it was not performed during the preprocessing.

- Topographic Correction: Slope, aspect and elevation effect the illumination as a result of the changing sun angle relative to the angle of the terrain. This can cause variation in reflectance values of similar ground features with different terrain characteristics. Topographic correction is applied to reduce these effects. There are various methods for this correction. The

simplest methods involve using band ratios, but they are found to be inferior to the complex methods that uses DEM to model the illumination effects taking into account terrain characteristics like slope and aspect. This correction is not always need but is particularly important for mountainous and rugged terrain (Bruce & Hilbert, 2006; Young et al., 2017).

The methods of topographic corrections are based on the modelling of illumination condition (IL) which is derived using parameters obtained from a DEM. It`s value lies between -1 and +1 indicating maximum and minimum illumination condition. It can be obtained using the following equation.

$$IL = cos\theta_p cos\theta_z + sin\theta_p sin\theta_z \cos(\emptyset_a - \emptyset_o)$$

Where:

ρ_λ = TOA planetary reflectance

θ_p= Slope angle

θ_z= Solar zenith angle

$\emptyset_a$= Solar azimuth angle

$\emptyset_o$= Aspect Angle

Once the IL is calculated, it can be used in different topographic correction models like Cosine correction, Sun-Canopy-Sensor, Dymond Shepherd correction and Minnaert correction (Pimple et al., 2017).

Topographic correction was particularly important in this study as shadows were adversely affecting the SI values. Even though most of the study has flat terrain, the northern portion of the study area had hills that were casting shadow on the ground. After applying and observing the results from

Cosine, Sun-Canopy-Sensor and Dymond Shepherd correction, Dymond Shepherd correction was selected for reducing the effects of topographic shadows because the Cosine and Sun-Canopy-Sensor model introduced extreme values in the image.

Dymond Shepherd correction is a simple and robust correction in which a simple physical model of vegetation reflectance for visible light is used to predict the reflectance values on the slopes. The vegetation reflectance on a slope using this method can be calculated as follows.

$$\rho_s = \frac{\cos i + \cos e}{\cos i_s + \cos e_s}\ \rho$$

(Dymond & Shepherd, 1999)

Where,

ρ_s = reflectance on a slope

i = = angle of incident

e = angle of exitance

i_s = angle of incident on a slope

e_s = angle of exitance on a slope

By assuming the view angle of 0, the correction parameters can be obtained from a DEM and image metadata. When view angle is 0, e equals to 0, i equals the solar zenith angle, e_s equals the slope, and $\cos i_s$ equals to the illumination condition (Hurni et al., 2017).

Figures 4 shows a portion of Landsat 8 of 2019 image where the forest area is affected by topographic shadows. Figure 5 shows the illumination condition at the time of sensing of the same portion where the darker parts represent low illumination due to the shadows and brighter parts represent the well illuminated parts. This illumination condition raster was used as input for the aforementioned topographic corrections. Figures 6, 7 and 8

show the true color image of the same portion after applying Dymond Shepard, Cosine and SCS corrections respectively. From these figures, it is evident that the result from the Dymond Shepard correction was moderate and produced a better-looking or more natural image. On the other hand, Cosine and SCS correction introduced some extreme values. Due to this reason results from Dymond Shepard correction were selected for further processing.

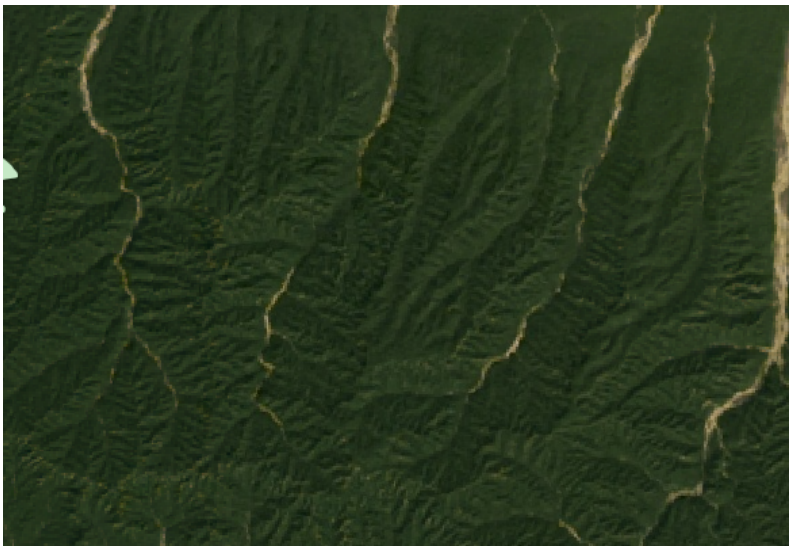

Figure 4: Landsat 8 true color image before topographic correction

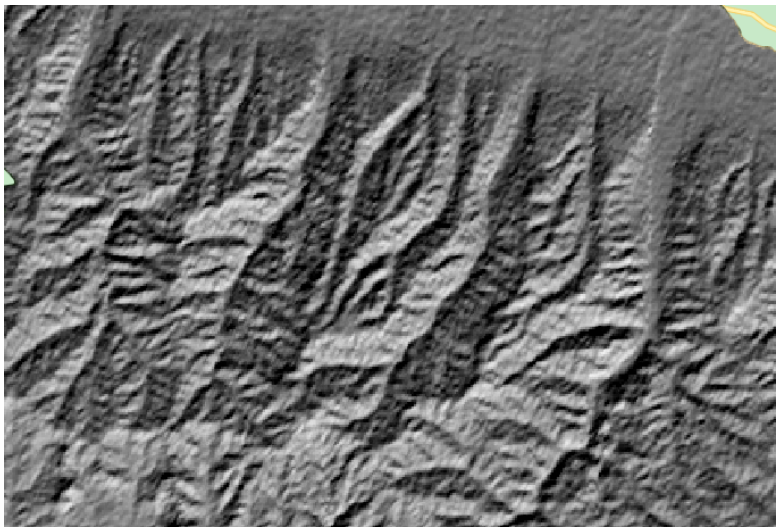

Figure 5: Landsat 8 image illumination condition

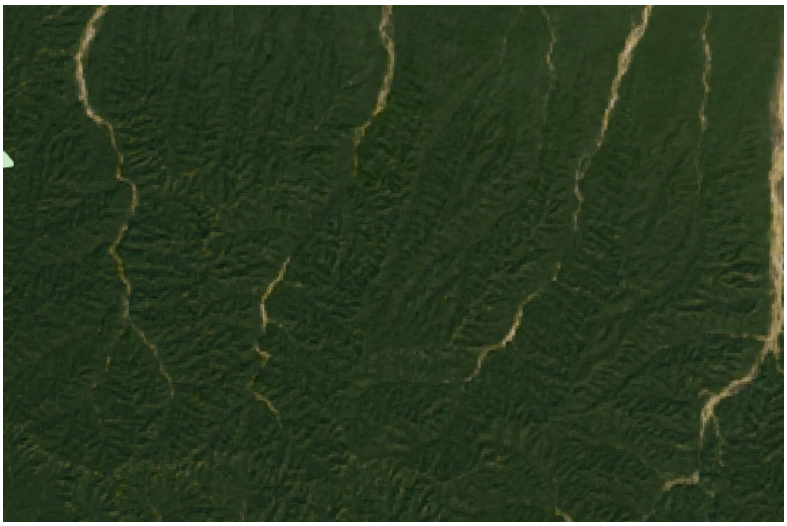

Figure 6: Landsat 8 true color image after Dymond Shepard correction

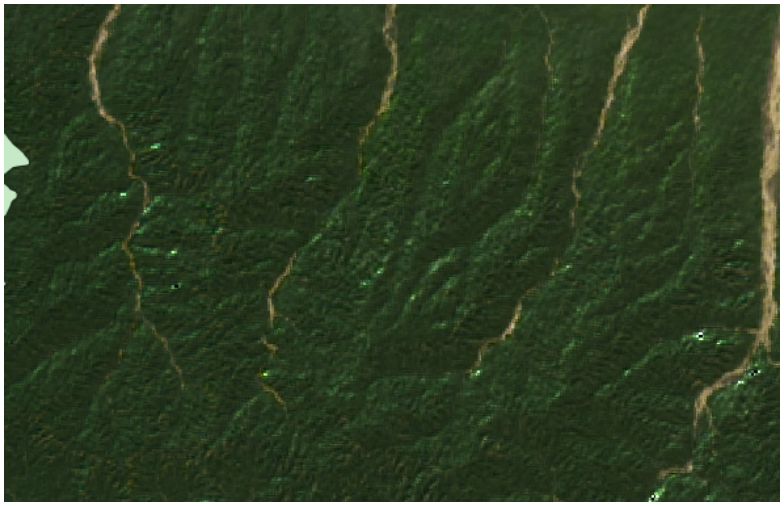

Figure 7: Landsat 8 true color image after Cosine correction

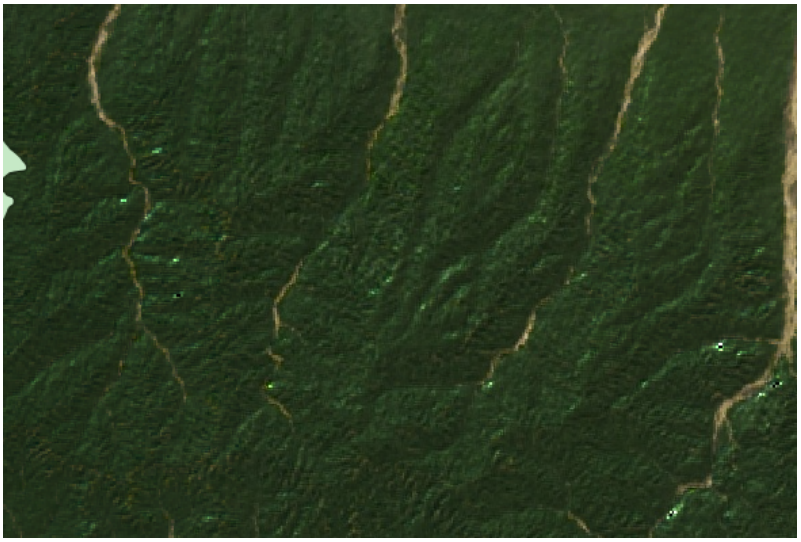

Figure 8: Landsat 8 true color image after SCS correction

iii. Atmospheric Correction: The energy captured by a sensor is affected by the atmospheric particles like gases, water vapor and aerosols due to scattering and

absorption. Atmospheric correction accounts for these effects. There are various methods for this correction, from simple dark object subtraction to complex method like Landsat Ecosystem Disturbance Adaptive Processing System (LEDAPS). Atmospheric correction is not always needed and can induce errors, thus should be avoided unless necessary. The images used in this study were already atmospherically corrected, thus this procedure was not performed.

This study uses Landsat 5 and Landsat 8 level-2 surface reflectance products. Both of the products are derived from Landsat Level-1 Precision and Terrain product (L1 TP) (Google Earth Engine, n.d.-a, n.d.-b). L1 TP are geometrically and radiometrically corrected using ground control points and DEM (USGS, n.d.). Landsat 5 Surface Reflectance are generated by using a specialized software called LEDAPS which applies atmospheric correction routines to Landsat 4-5 and Landsat 7 data. It generates TOA reflectance and TOA brightness temperature using calibration parameters from the metadata. Auxiliary data such as water vapor, ozone, atmospheric pressure, aerosol optical thickness, and DEM are then input with Landsat TOA reflectance and TOA brightness temperature to a model called Second Simulation of Satellite Signal in the Solar Spectrum (6S) radiative transfer model to generate the final surface reflectance product. Similar procedure is also applied to the Landsat 8 L1 TP products to obtain the Landsat 8 level-2 product using a software called Land Surface Reflectance Code (LaSRC) (USGS, 2020a, 2020b).

iv. Cloud, Cloud Shadow, Haze and Water Masking: Besides obscuring the ground and casting shadows, clouds and haze usually have high reflectance values than the ground which adversely affects the derived indices. Water on the other hand absorbs NIR radiation causing similar problem, thus they need to be removed beforehand.

The obtained images were cloud free, so cloud masking was not needed. But Figure 9 shows that the Landsat image of 2003-12-25 had some haze in the south-eastern part of the study area which adversely affected the SI values. Thus, for that portion of the image, median pixel values of 2003-12-09 and 2003-12-25 image was used which considerably reduced the haze. Figure 10 shows the effect of haze on SI.

Figure 9: Portion of image before (left) and after reducing the haze (right)

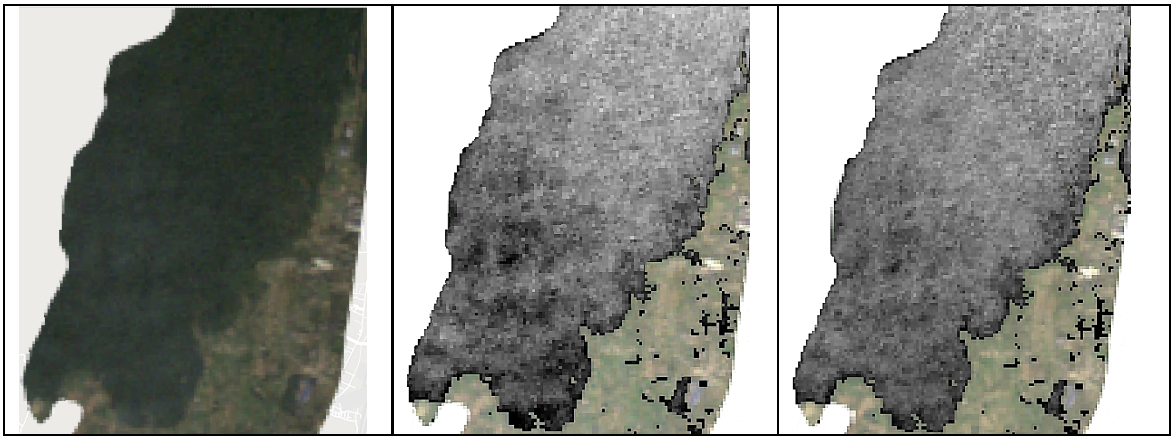

Figure 10: Portion of image with haze (left), SI index in the area (middle), SI index in the area after reducing haze (right)

The water bodies in the images were removed using Automatic Water Extraction Index (AWEI) proposed by Feyisa et. al (2014). In the raster produced using this index, water pixels have higher positive values and other pixels have values near 0 or negative. Thus, an appropriate threshold can be used to separate surface water from other land cover classes (see Figure 11). This index can be produced using the following formula.

$$AWEI = Blue + 2.5 \times Green - 1.5(NIR + SWIR1) - 0.25 \times SWIR2$$

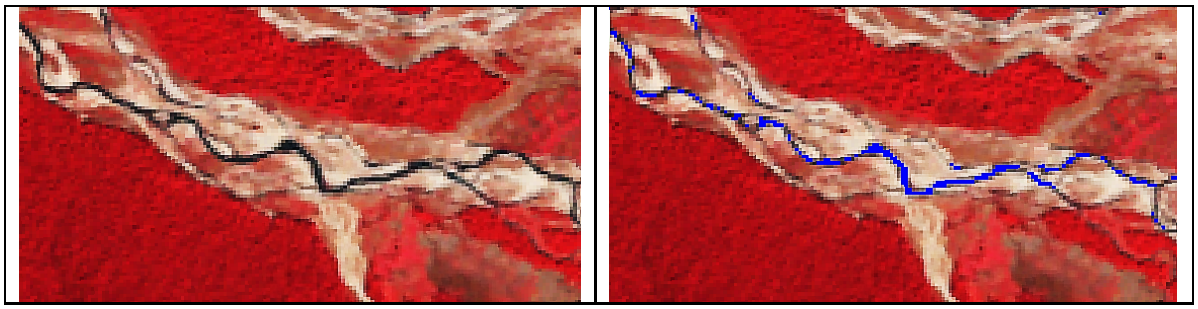

Figure 11: False color composite using NIR-Red-Green (left), water mask (blue) produced using AWEI (right)

2.4. Range Normalization

Range normalization is the process in which all the data is scaled between a common range of values to make them comparable. In this study, normalization is essential because later the indices derived using different bands will be integrated together to derive vegetation density raster and final FCC (ITTO & JOFCA, 1999).

A dataset can be rescaled by applying a transformation function to transform the values onto specified scale such as 0 to 1, -1 to 1, 0-100 etc. A transformation function is a mathematical function which can be used to transform the old values of a dataset into a desired scale. A variety of transformation function can be used while normalizing a dataset such as linear, exponential, logarithmic, gaussian, power etc., but a suitable transformation function is the one that captures the nature of the dataset or the phenomena which the dataset represents most appropriately (Esri, 2021a).

In this study, a linear transformation was done to rescale the band values into an 8-bits range i.e., from 0 to 255. In this transformation, dataset minimum and maximum are used to derive a linear function which is then used to transform the input values. In contrast to functions such as exponential function where the new values increase exponentially as the input values becomes larger, the new values in linear transformation increase or decrease at a constant linear rate. This makes linear transformation a good option for

normalization in this case because we want to preserve the original distribution of the values (Esri, 2021b).

2.5. Image Classification

Image classification is the simplification of the spectral information into a limited number of classes. It is a major product of satellite images, and is the basis of many environmental and socio-economic applications (Tupin et al., 2014). The general process of a satellite image classification includes selection of appropriate land cover classes, selection of training samples, training a classifier, accuracy assessment and post classification analysis. There are various approaches of image classification approaches like pixel based (per-pixel and sub-pixel), per-field based, object oriented, contextual and knowledge-based classification (Lu & Weng, 2007).

Pixel-based classification approaches classify pixels in an imagery solely based on their based on their spectral characteristics. Each pixel is assigned to a class based on their spectral similarity. In contrast to object-based methods, this approach does not take into account spatial or contextual properties (Yan et al., 2007). At the core of the image classification are the classifiers or the algorithms that classify the image based on some mathematical model. Commonly used classifiers include maximum likelihood, K-means clustering, ISODATA, support vector machine, random forest and artificial neural networks. There is no rule of thumb for selecting appropriate classification approach and classifiers for a specific study area, but some factors to consider include aim of the classification, heterogeneity of the study area, classification accuracy, classifier performance, effective separation of the classes and computational resources. But in general practice, researcher`s experience, available software, resolution of the satellite imagery, classification system, available ancillary data, time and cost all may affect the decision to some degree (Lu & Weng, 2007).

This study uses pixel-based classification approach using RF classifier for image classification. The workflow is given in the Figure 12 and the procedure is described in the following sub-headings.

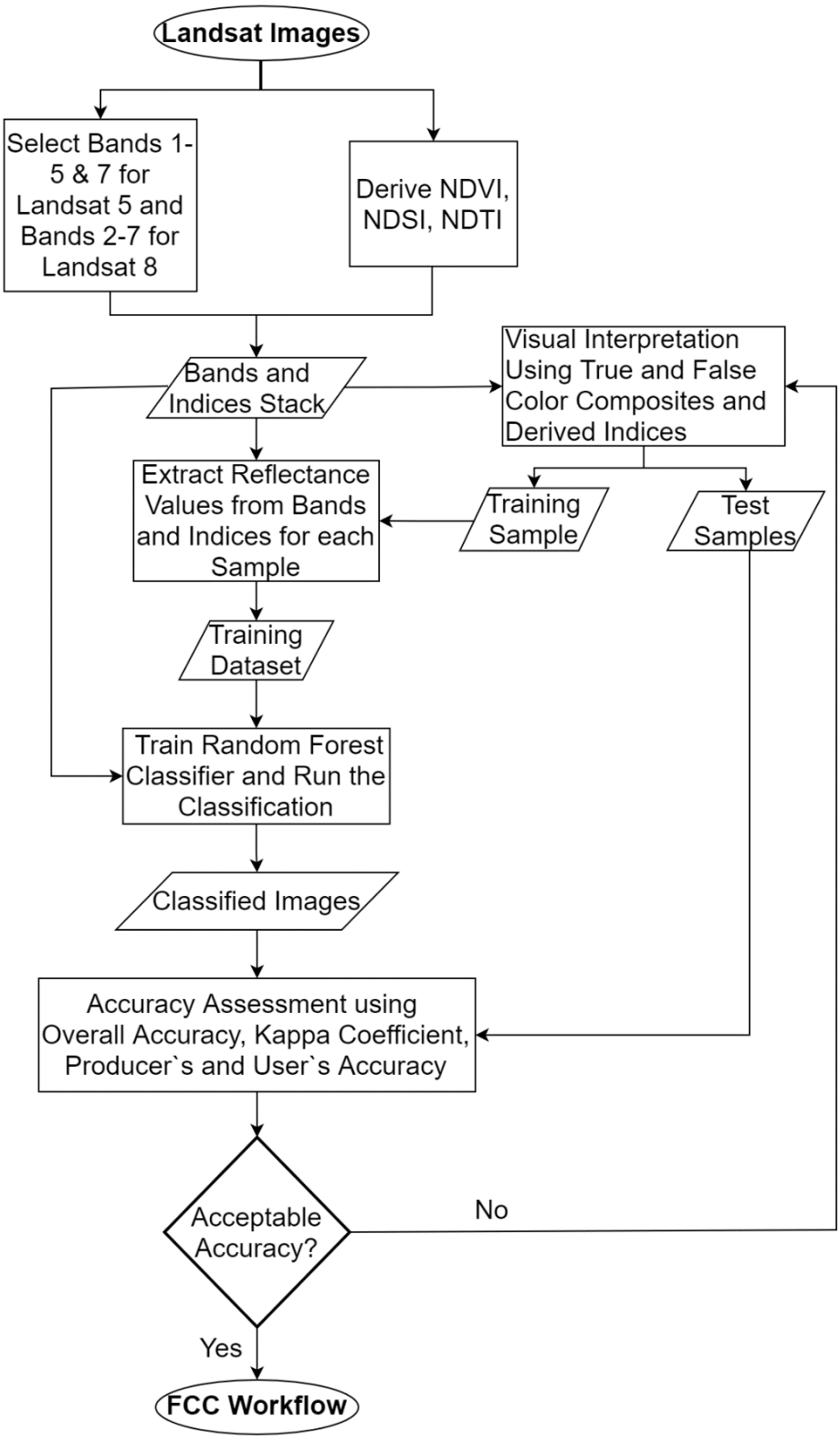

Figure 12: Image Classification Workflow

2.5.1 Selection of Classes

After observing the visible land cover classes in the satellite images, and due to the requirement of vegetation and forest mask in further processing procedures, a total of three land cover classes were selected in this study (see Table 3).

Table 3: Land Cover Classes

Classes	Description
Forest	Area covered with trees
Other Vegetation	Vegetation except forest including agriculture, grassland and other small vegetation
Non-vegetation	Bare land, built-up and water

2.5.2. Sample Collection for Training and Accuracy Assessment

Training samples were collected mostly using true color composite of the satellite images, but indices and false color composites (NIR-Red-Green) were also used where verification was necessary. Ideally a random sampling should be done, collecting abundant samples for each class that are representative of the entire study area (Millard & Richardson, 2015). But random sampling strategy was difficult to implement in this case due to lack of high-resolution imagery for verifying the samples. Thus, samples were collected, as far as possible, uniformly from all over the study area where classes could be identified from the Landsat images with some certainty. In the same way samples for accuracy assessment were also collected. No of samples used for training and testing is given in Table 4.

Table 4: Training and Testing Samples

	No. of Training Samples			No of Testing Samples		
Class	1989	2003	2019	1989	2003	2019
Forest	42	48	42	42	42	42
Other Vegetation	42	34	35	42	42	42
Non-Vegetation	42	42	30	42	42	42

2.5.3. Training the Classifier and Image Classification

Random Forest (RF) classifier in GEE was used to classify the images. RF is one of the most popular machine learning classifier. It is an ensemble of classification trees that uses a number of different base classifiers to perform multiple classification of the same data.

Then the final classification is selected on the basis of majority vote from all the classifiers. The principle behind this “Ensemble Learning” is based on the premise that a group of classifiers can produce better classification results than an individual classifier (Lu & Weng, 2007; Rodriguez-Galiano, Ghimire, et al., 2012).

RF classifier requires user to define two parameters to generate the decision trees and predictions- the number of desired classification trees to be used for final voting, and the number of prediction variables used in each node. The decision trees used in the classification are grown from randomly generated subset of training samples, and each tree is grown from different sets of sub-samples through a technique called bagging or bootstrap. In this technique, random sub-sample are generated from training samples with replacement i.e., selected training sub-samples are not deleted. Therefore, some training samples may be used more than once which makes it more robust when facing slight variations in the input samples and at the same time increases accuracy. Bagging also makes RF classifier significantly less sensitive to noise and overtraining (Rodriguez-Galiano, Chica-Olmo, et al., 2012; Rodriguez-Galiano, Ghimire, et al., 2012). The collected training samples were used to extract the values from the selected bands and indices, which was then used to train the Random Forest (RF) classifier and perform the classification. A total of 200 decision trees were used to classify the images.

2.6. Forest Canopy Cover

The methodology to derive FCC in this study is based on Rikimaru`s (1996) FCD model. However, the FCD model has been modified in order to increase accuracy of the derived results and reduce user`s subjectivity in identifying vegetation and forest land covers. In the FCD model, the vegetation and bare land in the study area is differentiated by thresholding a vegetation index and BI respectively. Similarly, forest mask is derived integrating a vegetation index, SI and BI. FCD model uses TI and vegetation index to identify the forest gaps and black soil. These things make the FCD model more

subjective, thus in this study, vegetation and forest masks are obtained through supervised image classification. Furthermore, supervised image classification also eliminates the need for identifying forest gaps and black soil. The workflow to derive FCC is given in Figure 3 and the procedure is discussed in the following headings.

2.6.1. Indices Used to Derive Forest Canopy Cover

In this study, NDVI, BI and SI were used to derive FCC. NDVI was selected instead of AVI because of its very strong negative correlation with BI. Details regarding the indices is given in the following headings and the observed relationship between the indices is given in figures 13, 14, 15 and Table 5.

i. NDVI

Chlorophyll in vegetation absorbs red light whereas the mesophyll cells in vegetation scatter/reflect the NIR light. This spectral characteristic of vegetation is the basis for deriving NDVI and numerous other vegetation indices. NDVI is derived using the red and NIR bands of Landsat. It is the most widely used vegetation index used to study biophysical properties of vegetation such as leaf area index, biomass and vegetation density. Since NDVI has a positive relationship with vegetation density, in this study, it is used to derive vegetation density (VD) (Gitelson, 2004; Jiang et al., 2006; Purevdorj et al., 1998).

$$NDVI = \frac{NIR - Red}{NIR + Red}$$

ii. BI

NDVI is not very reliable when soil under a forest canopy is exposed to a higher degree, thus relationship between NDVI and BI was used to estimate the vegetation density. BI value increases as the amount of soil increases and vice versa (Rikimaru et al., 2002). The formula to derive BI is given below.

$$BI = \frac{(SWIR1 + Red) - (NIR + Blue)}{(SWIR1 + Red) + (NIR + Blue)} \times 100 + 100$$

iii. SI

SI provides information on structure of the canopy based on the shadow casted by the trees. SI quantifies the shadows based on the fact that shadows have low reflectance values in the visible bands. SI values are based on the amount of trees rather than amount of all vegetation. It is an important factor in FCC mapping because NDVI saturates earlier than SI, thus might not represent the canopy cover appropriately (ITTO & JOFCA, 1999). The formula to derive SI is given below.

$$SI = \sqrt[3]{(256 - Blue) \times (256 - Green) \times (256 - Red)}$$

2.6.2. Relationship between the Indices

For better FCC estimation, ideally, when NDVI increases BI should decrease and vice versa. Also, SI should increase when NDVI increases. The FCC model utilizes these relationships to predict the per-pixel FCC values for each Landsat image. Figures 13, 14, 15, and Table 5 confirms these relationships, which indicates that safe integration of the indices to estimate FCC is possible.

The scatterplots given below show how the indices are related to each other, the trend line shows the modelled relationship and R^2 indicates how well the data follows the model. Table 5 shows how strongly the indices are related to each other. From the figures and the table, it can be observed that NDVI and SI have strong positive correlation, whereas both NDVI and SI have a strong negative correlation with BI.

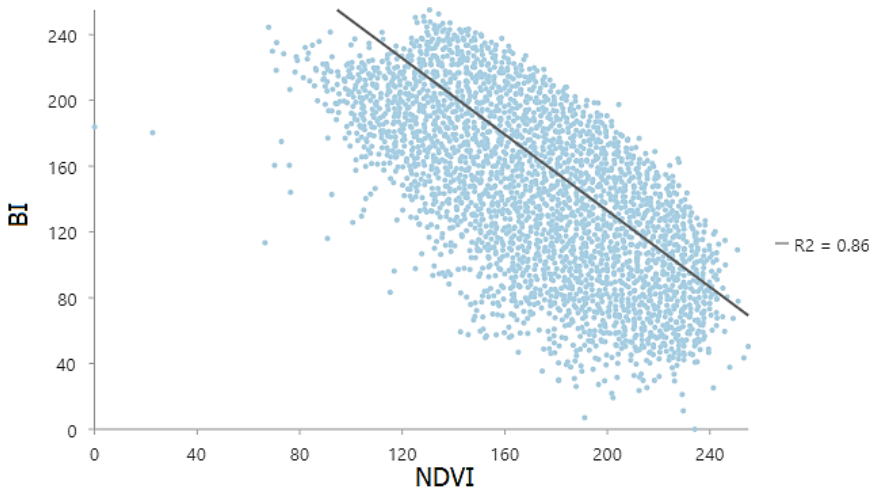

Figure 13: Relationship between NDVI and BI

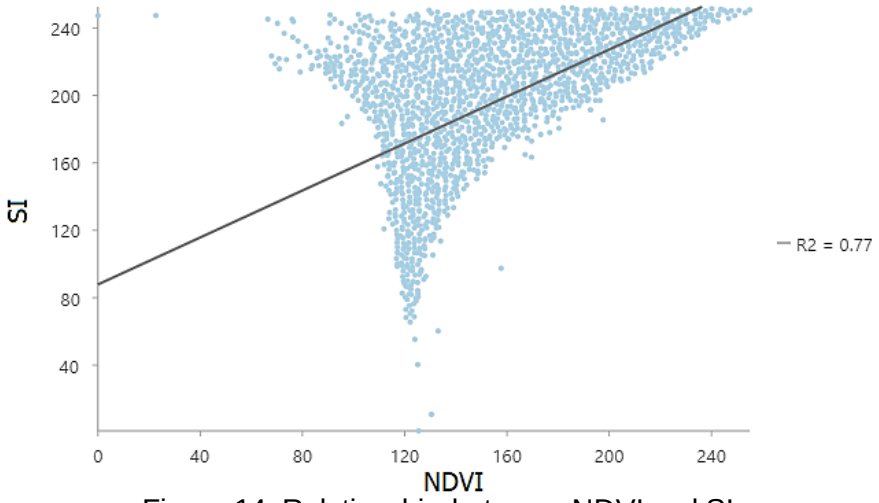

Figure 14: Relationship between NDVI and SI

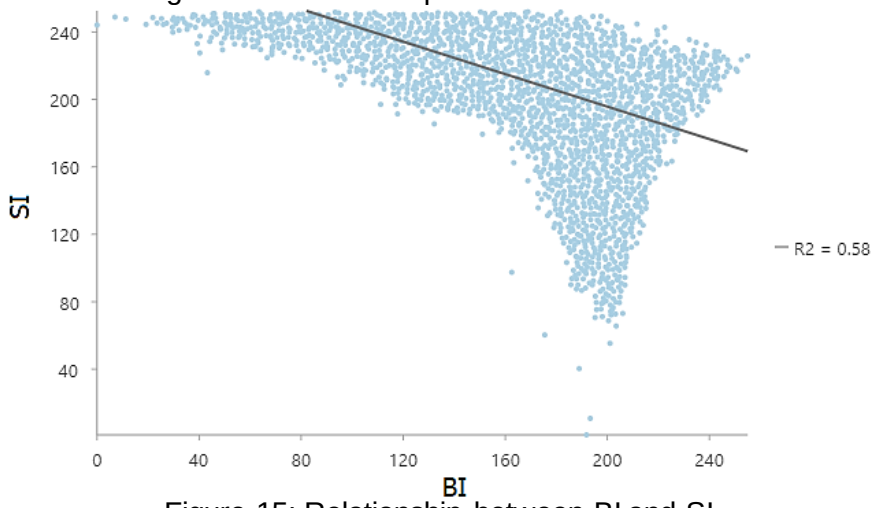

Figure 15: Relationship between BI and SI

Table 5: Corelation Matrix-NDVI, BI and SI

Indices	NDVI	BI	SI
NDVI	1	-0.927	0.879
BI	-0.927	1	-0.759
SI	0.879	-0.759	1

2.6.3. Deriving Vegetation Density

NDVI is positively correlated to vegetation density, but NDVI values are also affected by the exposed soil in case of mixed pixels. Thus it becomes necessary to account for the effect of bare soil while deriving vegetation density (Rikimaru et al., 2002; Xue & Su, 2017).

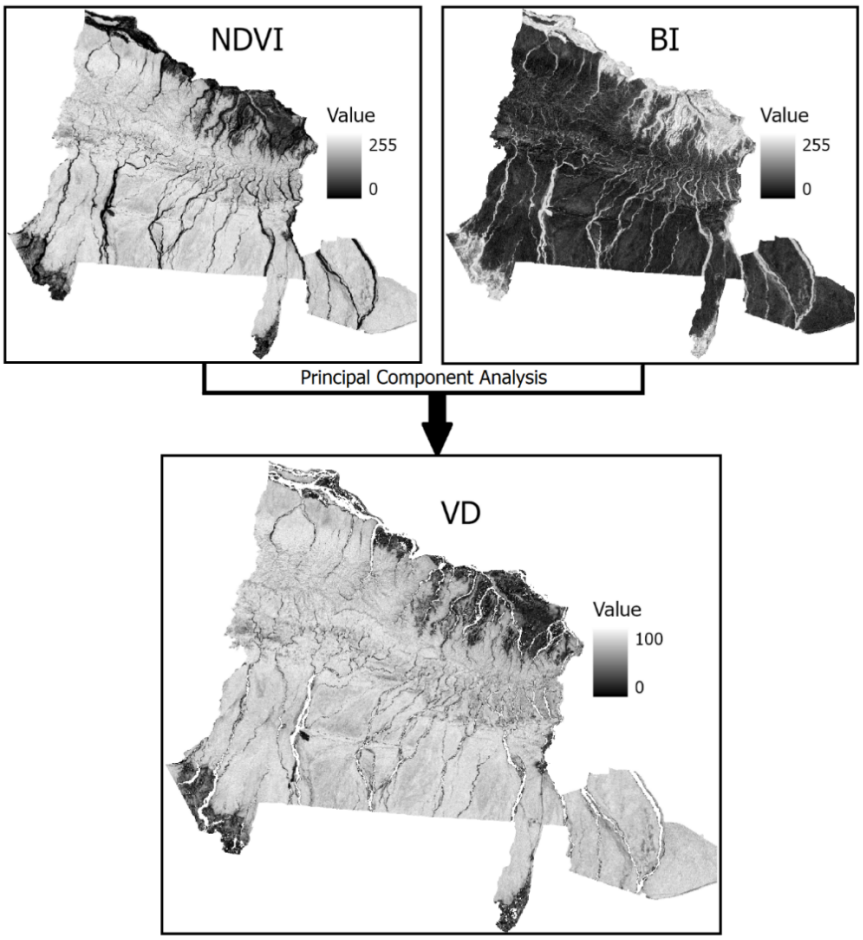

Figure 16: Deriving vegetation density

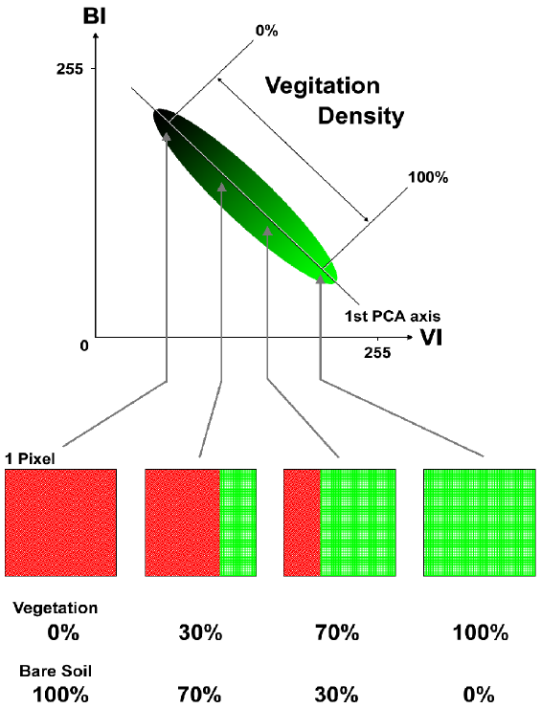

Figure 17: Concept of VD

In this study, NDVI and BI were integrated together using Principal Component Analysis (PCA). The first principal component from the PCA was then rescaled from 0 (representing pure bare soil pixel) to 100 (representing pure vegetation pixel) to get the vegetation density raster. Figure 17 illustrates the concept of VD as given by Rikimaru (1996). The procedure to derive vegetation density using NDVI and BI through PCA is described in the following headings.

i. Confirming the conditions for integration

Since we are integrating a vegetation index and BI to derive vegetation density, it is very important that the indices are strongly correlated (ITTO & JOFCA, 1999). Thus prior to PCA, correlation analysis between AVI and BI, and NDVI and BI was done. Results from the correlation analysis revealed that AVI and BI are less correlated than NDVI and BI in case of all the images, thus NDVI was selected for the PCA.

ii. Principal Component Analysis

PCA is the most widely used statistical technique for reducing data dimensionality while preserving as much information or variability as possible. PCA is used to analyze several, usually correlated datasets to extract important information in the form of principal components. The fundamental principal in PCA is to find a new spectral space where the datasets do not have any correlation or the covariance matrix of the new dataset is a diagonal matrix. In finding this new dataset, a linear combination of the original datasets accounting for the maximum variation of the pixel values in each dataset is identified. This new dataset is a multiband band image, and each band is called a principal component. There are as many principal components as there are no. of datasets used in the PCA. The first band or the first principal component of this new dataset explains majority of variation in the original datasets (Abdi & Williams, 2010; Rodarmel & Shan, 2002). Figure 18 given by Richards (2013) illustrates how data correlated in one spectral space can be uncorrelated in a new spectral space.

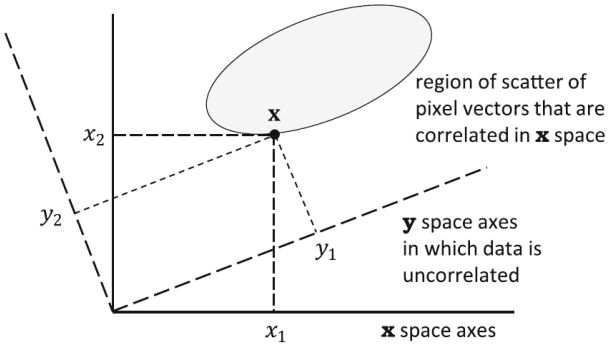

Figure 18: Concept of PCA

The general steps to carry-out PCA involves deriving covariance matrix of the datasets (in this case NDVI and BI), determining the eigen values and eigen vectors of the covariance matrix and finally forming the principal components using the eigen vectors as the weighing coefficients (Richards, 2013). The procedure for PCA as given by Richards (2013) is discussed in the following paragraphs.

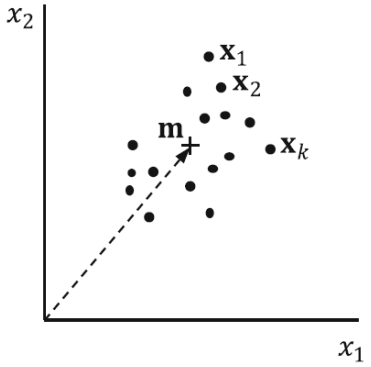

Figure 19: 2-D spectral space

As seen in the figure 20, suppose x represents pixels in a spectral space with two spectral components/dimensions showing individual pixel vectors and their average (m). Then, the covariance matrix of the datasets is given by the following equation.

$$C_x = \varepsilon\{(x-m)(x-m)^T\}$$

Where,

ε = Expected or average value of the pixel vector

x = Pixel vector

$m = \epsilon\{x\} = \frac{1}{k}\sum_{k=1}^{k} x_k$ (where x_k are the individual vectors of total no. K)

T = Vector transpose

Using the covariance matrix eigen values can be derived using the following equation.

$$|C_x - \lambda I| = 0$$

Where,

C_x= Covariance matrix

λ= Eigen value

I= Identity matrix

Solving the above equation leads to a quadratic equation from which eigen values can be derived. Eigen values are then used to derive the eigen vectors using the following equation.

$$|C_x - \lambda I|G = 0$$

Where, G is the transposed eigen vector matrix. Finally principal components can be derived using the eigen vectors and the original pixel values using the following equation.

$$y = Gx$$

Where,

y= Vectors describing the pixel points in new spectral space.

The above equation says that each component of y is a linear combination of all the elements x, and the weighing coefficients are the elements of the matrix G.

After obtaining the principal components, the first principal component was used to derive the VD. The first principal component was rescaled from 0 to 100% inside the vegetation land cover (including forest) through linear transformation to obtain the VD (see Figure 18).

2.6.4. Deriving Scaled Shadow Index

VD can adequately represent FCC in case where there is bare ground underneath the canopy. But in situations where the FCC is low and there is presence of undergrowth, VD overestimates the FCC as it is the percentage of area covered by vegetation (all types of vegetation including forest). Thus, to distinguish between the undergrowth and the forest canopy SSI is used in the final integration model. SSI is obtained by linear transformation of SI in the forest area, and like VD, SSI is also scaled from 0%-100%. A forest area having SSI of 0% indicates that the area has lowest possible shadow value, whereas SSI of 100% means the forest area has highest possible shadow (Rikimaru et al., 2002).

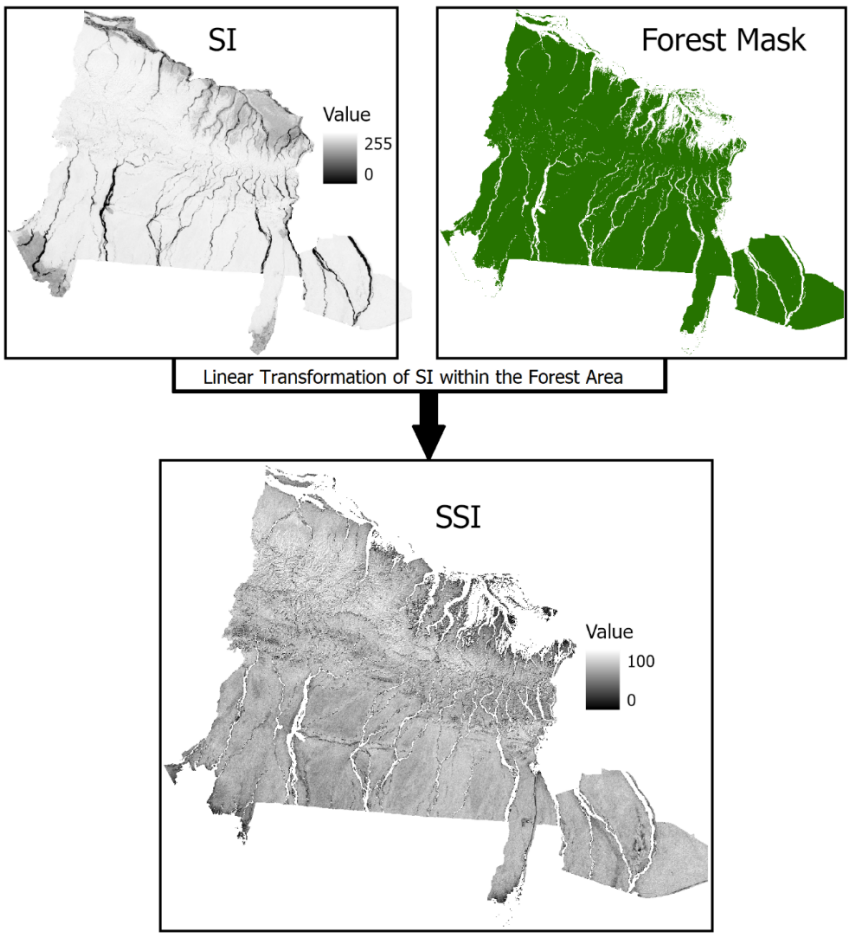

Figure 20: Deriving scaled shadow index

2.6.5. Deriving Forest Canopy Cover

Integration of SSI and VD is important to distinguish between the tree canopy and undergrowth. Thus, VD and SSI are integrated together to give a reliable estimate of FCC

(Rikimaru, 1996). VD and SSI are integrated together to derive FCC using the following equation.

$$FCC = \sqrt{VD \times SSI + 1} - 1$$

The observed relationship between VD, SSI and FCC derived from Landsat 5 image of 1989 is given in the figures 21, 22, 23 and Table 6. The colors red to green through yellow represent the FCC values in ascending order. The figures and table indicate that all the variables have very strong positive correlation. In other words, FCC increases when VD and SSI increase and vice versa.

Table 6: Correlation matrix- VD, SSI and FCC

Indices	VD	SSI	FCC
VD	1	0.79	0.87
SSI	0.79	1	0.98
FCC	0.87	0.98	1

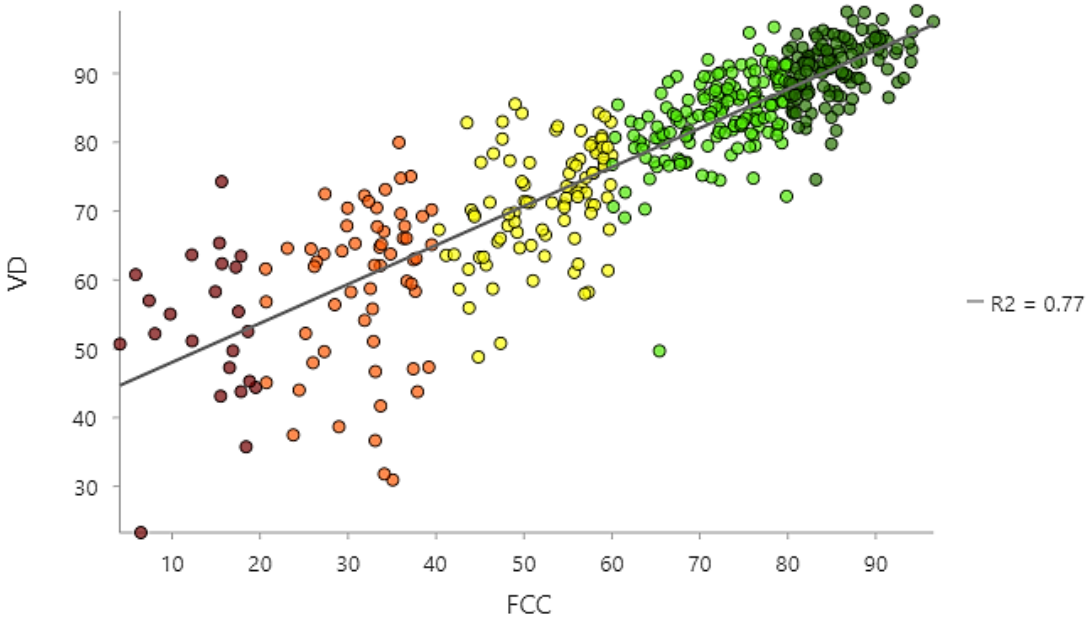

Figure 21: Relationship between canopy density and vegetation density

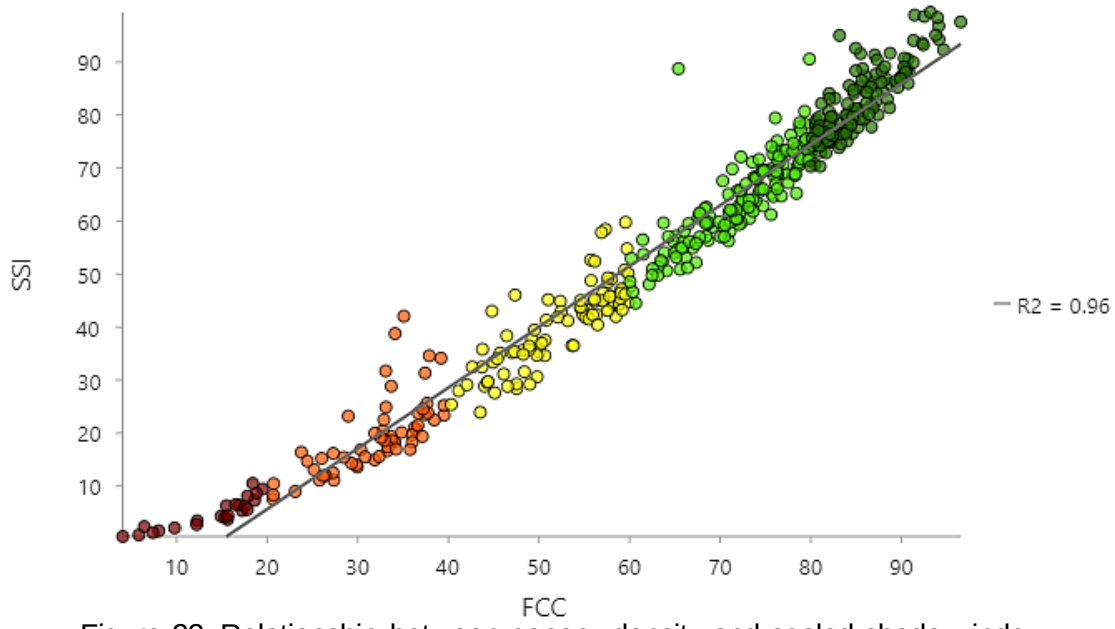

Figure 22: Relationship between canopy density and scaled shadow index

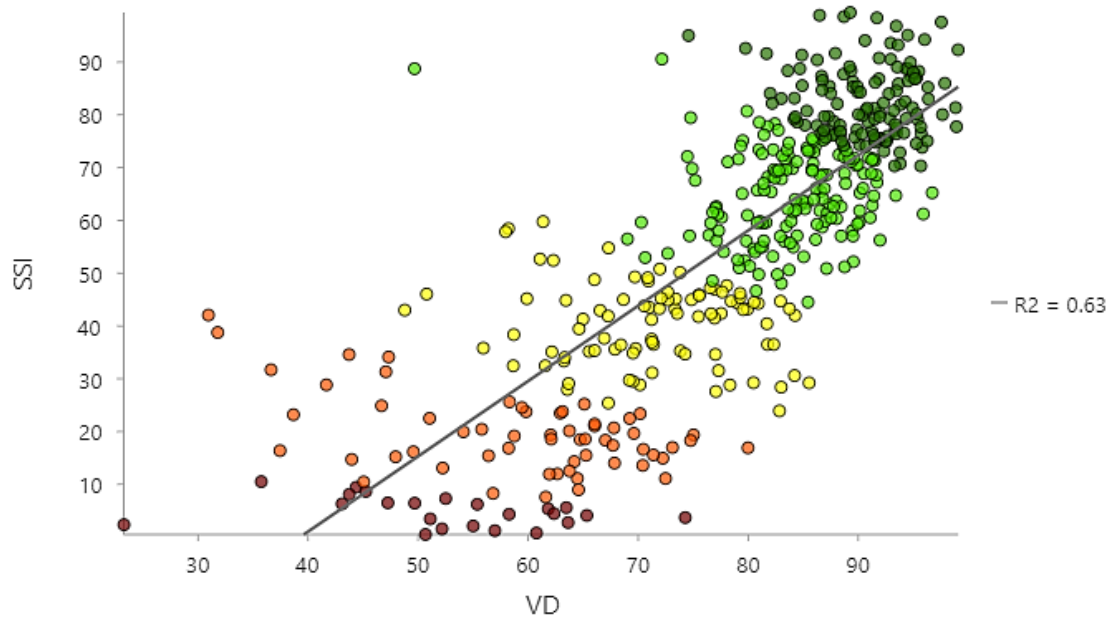

Figure 23: Relationship between vegetation density and scaled shadow index

Chapter Summary

In this study, Rikimaru`s (1996) FCD model with some modifications was used to estimate the FCC for 1989, 2003 and 2019. After the estimation, FCC change was studied using overlay operations and various statistics. In contrast to the FCD model where the vegetation, bare land and forest land cover classes were separated using thresholds, in this study, supervised image classification using RF was done to separate them in order

to increase the accuracy and reduce subjectivity. Initially, to prevent overestimation of FCC values, topographic correction using Dymond Shepard method was performed for the satellite images and haze in the 2003 image was reduced. Besides that, water bodies were also removed, and range normalization was performed to make the bands comparable and enable safe integration of the derived indices later.

After the initial processing, NDVI, BI and SI were derived using the pre-processed Landsat images. Then NDVI and BI were integrated through PCA to derive VD raster, and SI inside the forest area was rescaled from 0 to 100% to produce SSI raster. Both VD and SI rasters (scaled from 0 to 100%) were integrated together using the equation given by Rikimaru (1996) to derive the final FCC rasters. Finally, spatio-temporal change including intensity of change was studied and documented using FCC maps, various statistics, charts and tables.

Chapter-3: Results

3.1. FCC Status in 1989, 2001 and 2019

In 1989, out of the total forest area i.e., 80615.7 ha, majority (63.54%) of the park was covered by 60.1-80% class, while 80.1-100% class existed mostly in the northern part covering 21.71% of the park. The classes 40.1-60%, 20.1-40% and 0-20% covered 9.71%, 3.42% and 1.63% of the total forest area respectively. Most of the forest area near the settlements belonged to 40-60% or below that. The status of FCC in 1989 is given in Map 3 and table 7.

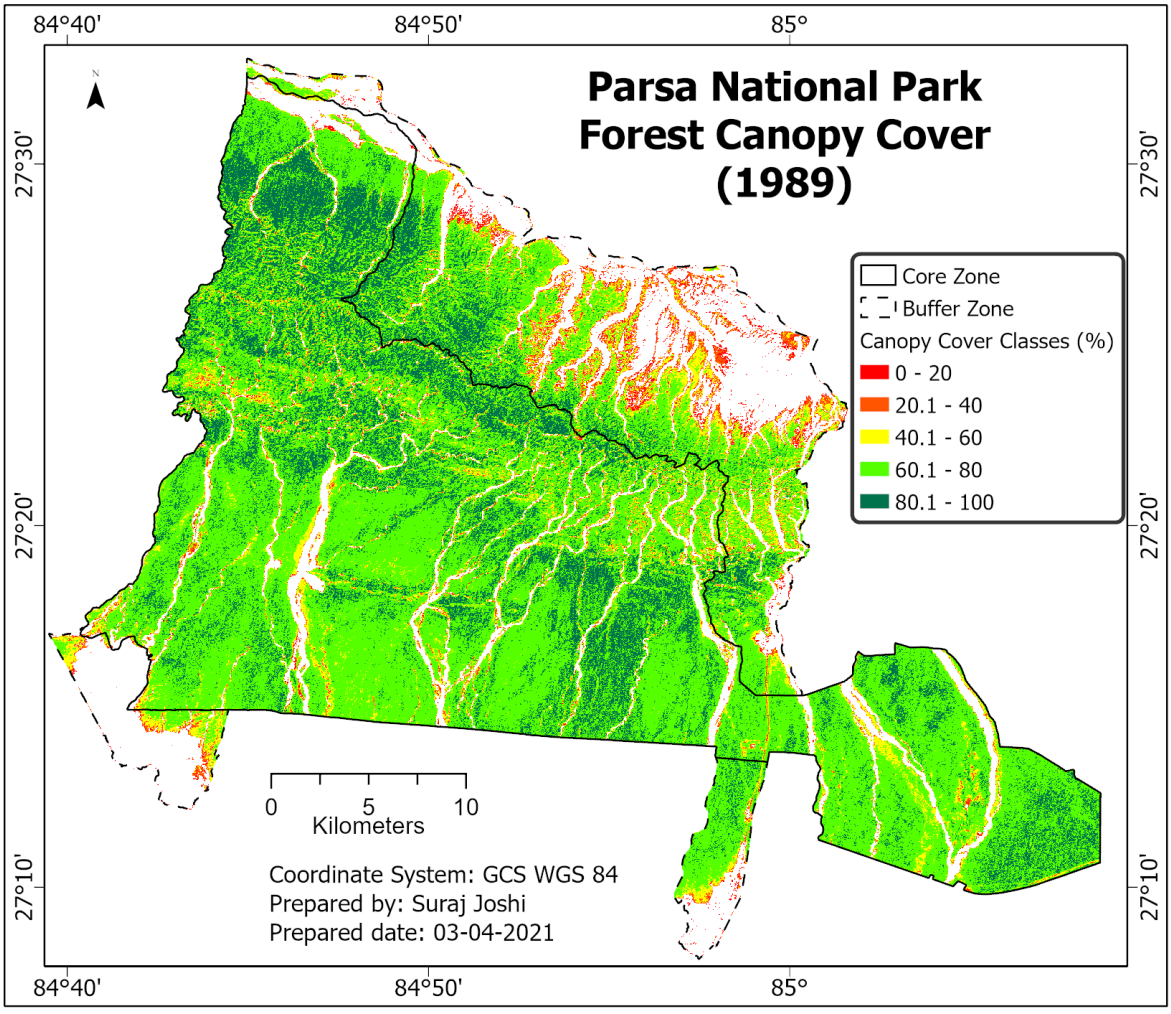

Map 3: Parsa national park canopy cover (1989)

Table 7: FCC status 1989

	Core Zone		Buffer Zone		Whole Park	
Classes	Area (ha)	Area (%)	Area (ha)	Area (%)	Area (ha)	Area (%)
0-20	395.1	0.63	916.2	5.26	1311.3	1.63
20.1-40	1203.0	1.90	1552.4	8.92	2755.4	3.42
40.1-60	4571.6	7.23	3255.3	18.70	7826.9	9.71
60.1-80	42296.3	66.92	8928.0	51.29	51224.3	63.54
80.1-100	14742.7	23.32	2755.1	15.83	17497.8	21.71
Total	63208.8	100.00	17406.9	100.00	80615.7	100.00

In 2003, out of the total forest area i.e., 79800.7 ha, half of the forest area was covered by 60.1-80% class, while 80-100% class covered 33.82% of the forest area. The classes 40.1-60%, 20.1-40% and 0-20% covered 10.86%, 4.10% and 1.93% of the total forest area respectively. Similar to 1989, most of the forest area near the settlements belonged to 40-60% or below that. The status of FCC in 2003 is given in Map 4 and Table 8.

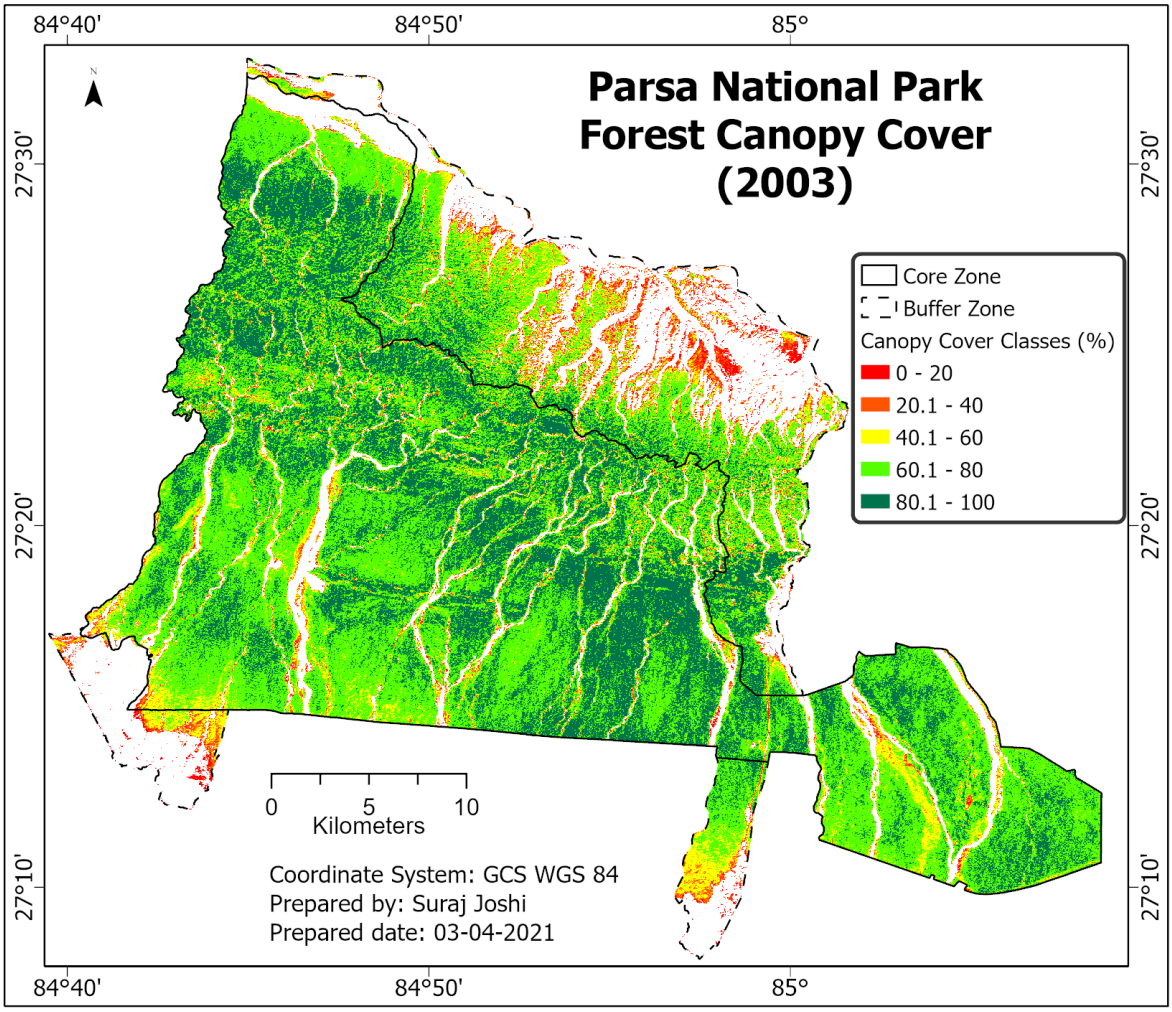

Map 4: Parsa national park canopy cover (2003)

Table 8: FCC status 2003

	Core		Buffer		Whole Park	
Class	Area (ha)	Area (%)	Area (ha)	Area (%)	Area (ha)	Area (%)
0-20	431.8	0.69	1107.2	6.56	1539.0	1.93
20.1-40	1341.6	2.13	1933.7	11.46	3275.3	4.10
40.1-60	5055.2	8.03	3614.6	21.41	8669.8	10.86
60.1-80	32357.1	51.43	6974.5	41.32	39331.5	49.29
80.1-100	23734.7	37.72	3250.4	19.26	26985.1	33.82
Total	62920.4	100.00	16880.3	100.00	79800.7	100.00

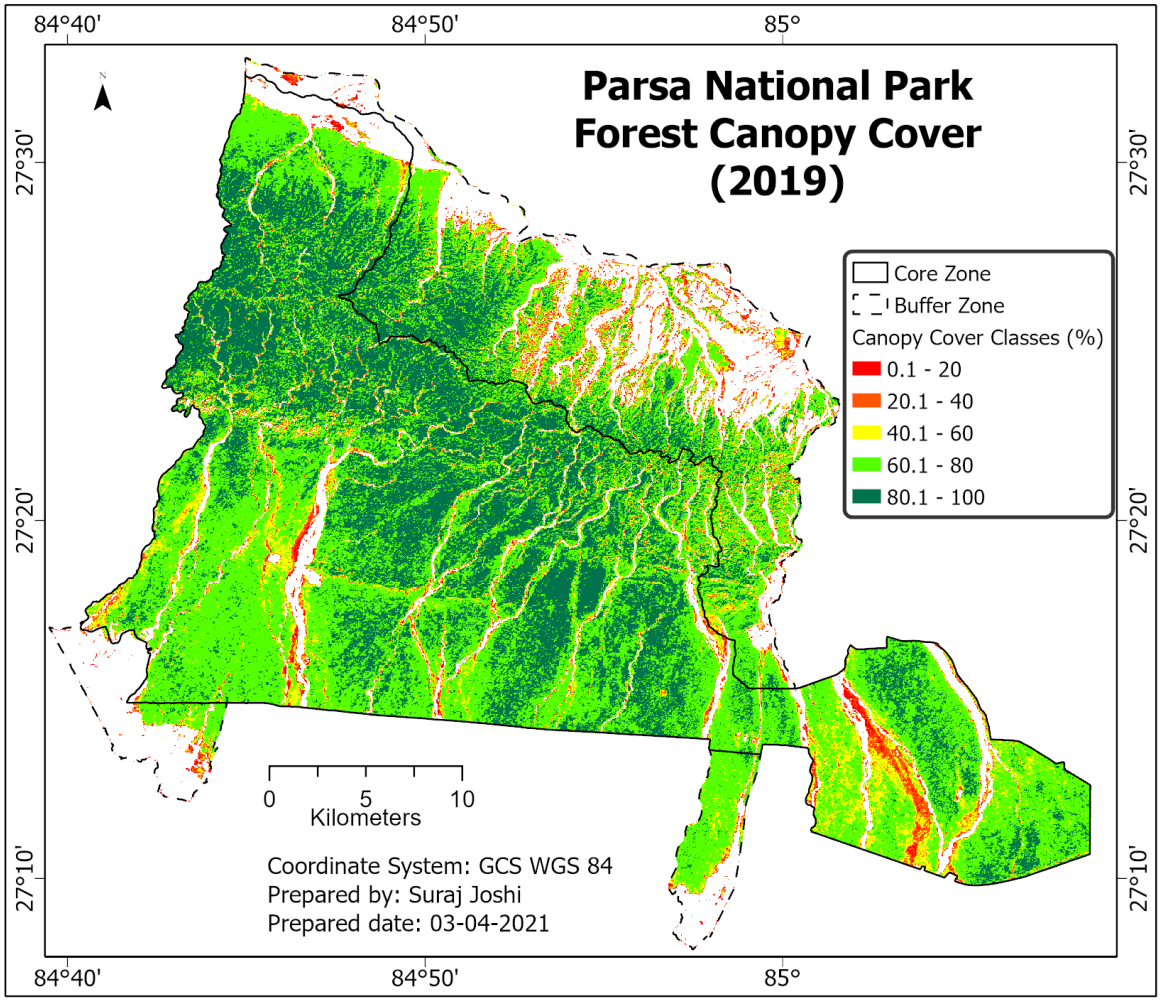

Map 5: Parsa national park canopy cover (2019)

Similar to 2003, in 2019, out of the total forest area i.e., 80817.8 ha, half of the forest area is covered by 60.1-80% class, while 80-100% class covers 34.41% of the forest area. The classes 40.1-60%, 20.1-40% and 0-20% covered 9.73%, 3.96% and 1.78% of the total

forest area respectively. In contrast to 1989, most of the forest area near the settlements belonged to 40-60% or above that. The FCC status in 2019 is given in Map 5 and Table 9.

Table 9: FCC status 2019

	Core Zone		Buffer Zone		Whole Park	
Class	Area (ha)	Area (%)	Area (ha)	Area (%)	Area (ha)	Area (%)
0-20	730.1	1.15	710.0	4.10	1440.1	1.78
20.1-40	1808.1	2.85	1392.6	8.05	3200.7	3.96
40.1-60	5355.1	8.43	2506.1	14.49	7861.2	9.73
60.1-80	32043.2	50.45	8466.9	48.94	40510.1	50.13
80.1-100	23580.4	37.12	4225.3	24.42	27805.7	34.41
Total	63516.8	100.00	17300.9	100.00	80817.8	100.00

3.2. FCC Change

Most of the change in FCC is seen in the higher classes i.e., 60.1-80% and 80.1-100% (see Figure 24). The 60.1-80% class has drastically decreased by about 11892.8 ha (14.25%) from 1989-2003, whereas 80.1-100% class has drastically increased by 9487.3 ha (12.11%) from 1989-2003. The 80.1-100% class has also increased from 2003 to 2019, thus showing an increasing trend. The 60.1-80% has also increased from 2003 to 2019, but the increase is very low as compared to how much it has lost from 1989 to 2003. All the other classes have increased from 1989 to 2003 and then have decreased from 2003-2019, but not significantly.

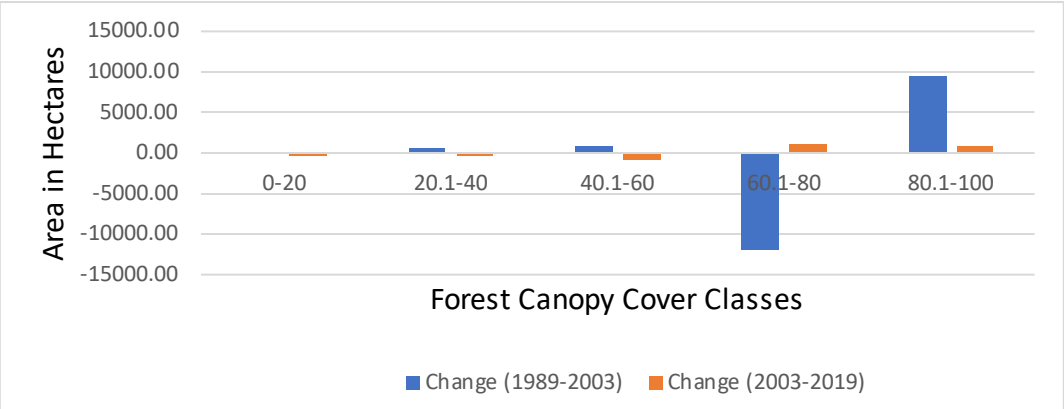

Figure 24: Canopy cover change (1989-2019)

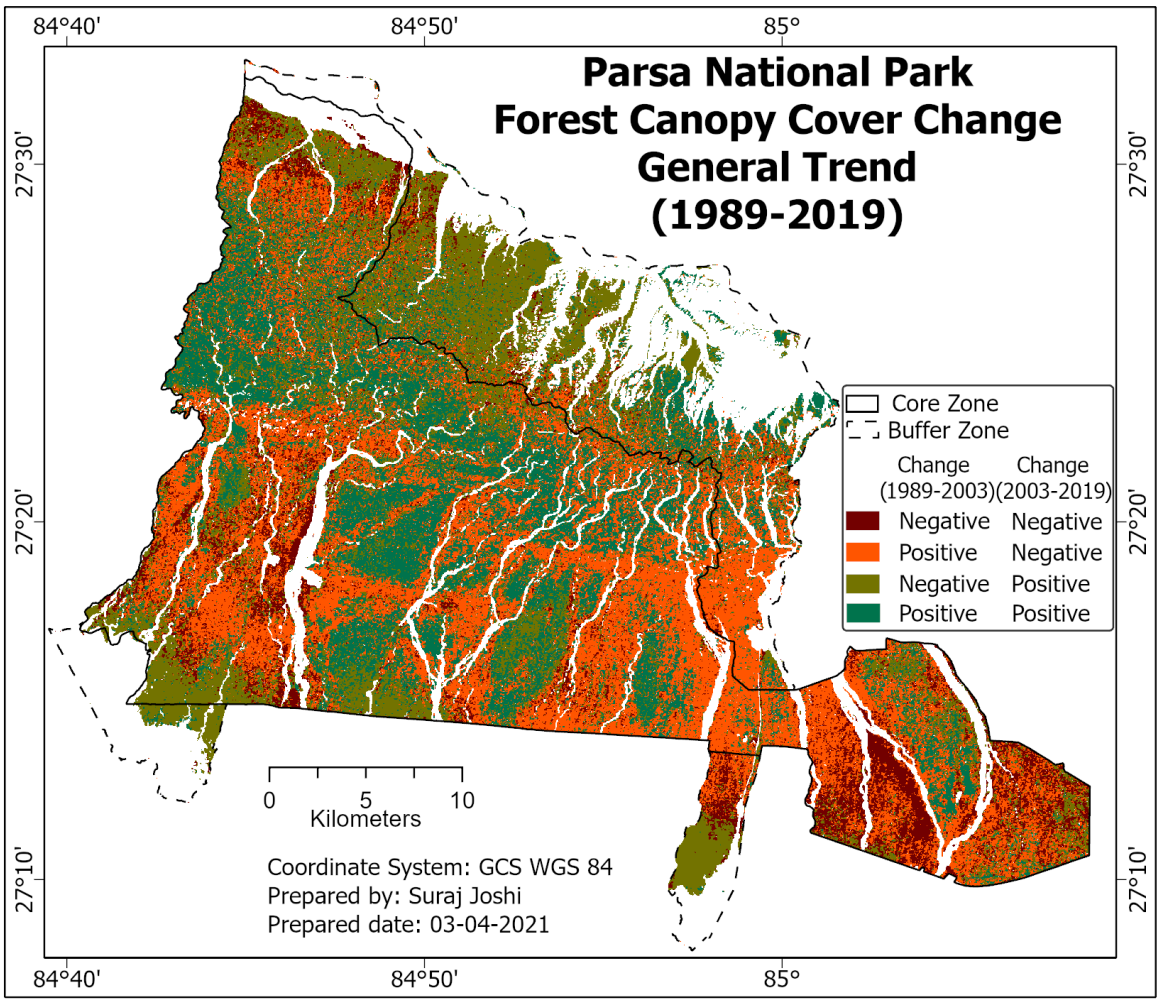

Map 6: Parsa national park canopy cover change trend (1989-2019)

In general, FCC in majority of the core zone seems to have positive change from 1989 to 2019, whereas majority of the forest in buffer zone have negative change from 1989 to 2003 and positive change from 2003 to 2019. Most of the forest area in the Churia region (hills in the northern part) and it`s foothills have positive change in FCC in both the time periods i.e., 1989-2003 and 2003-2019, whereas some portion of the extended part of the park has negative FCC change in both the time periods. Besides that, some portions of the forest area in near the settlements, major highways and the areas near stream have negative FCC change in both time periods. The general trend of FCC change from 1989 to 2019 is given in Map 6.

3.2.1. FCC Change (1989-2003)

From 1989 to 2003, the 60.1-80% class has drastically decreased by 14.25%, whereas the 80.1-100% class has drastically increased by 12%. FCC changes in all the other classes was found to be negligible. The change in different FCC classes from 1989 to 2003 is given in Table 10.

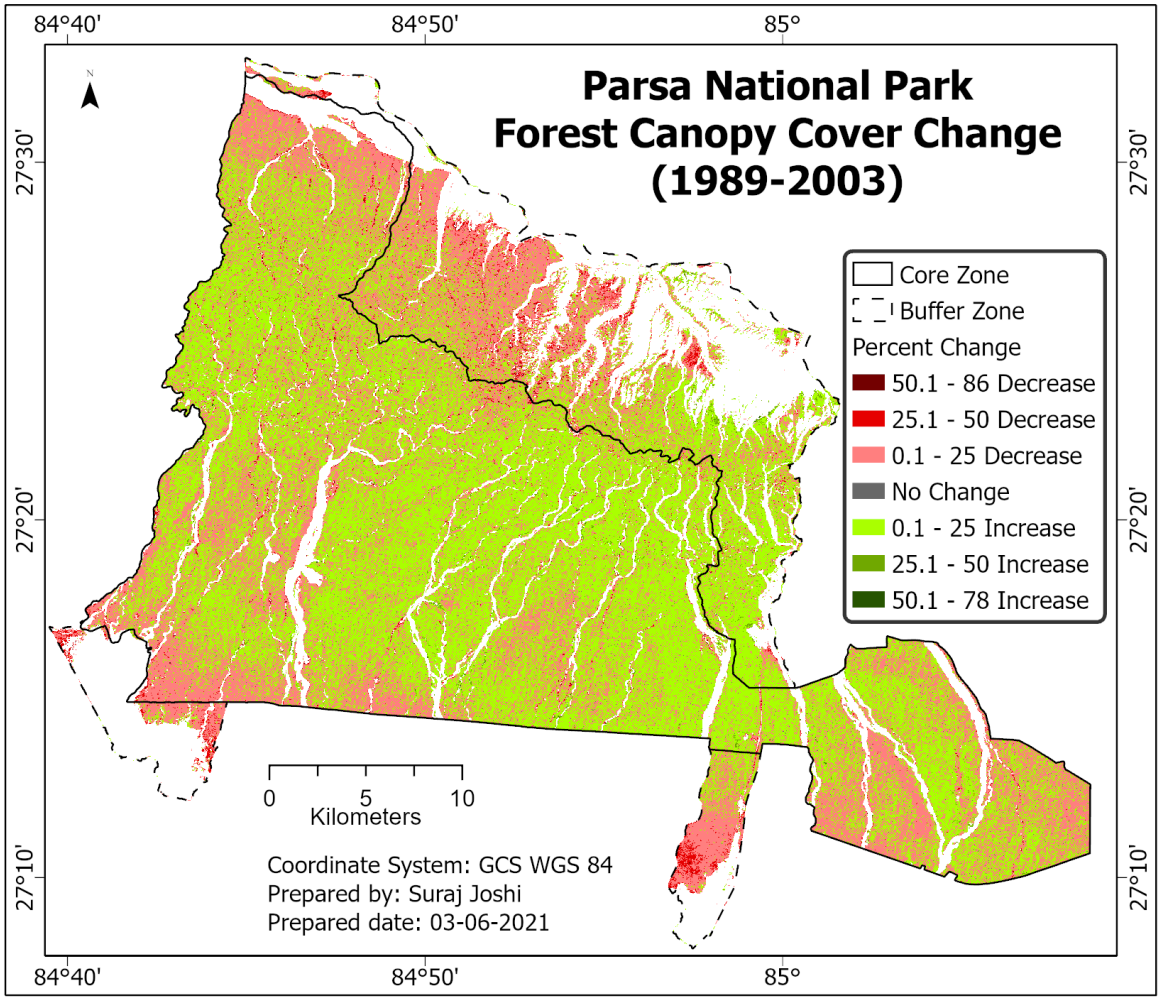

Map 7: Parsa national park canopy cover change (1989-2003)

Table 10: FCC change from 1989 to 2003

	1989		2003		Change 1989-2003	
Class	Area (ha)	Area (%)	Area (ha)	Area (%)	Area (ha)	Area (%)
0-20	1311.3	1.63	1539.0	1.93	227.7	0.30
20.1-40	2755.4	3.42	3275.3	4.10	519.84	0.70
40.1-60	7826.9	9.71	8669.8	10.86	842.94	1.15
60.1-80	51224.3	63.54	39331.5	49.29	-11892.8	-14.25
80.1-100	17497.8	21.71	26985.1	33.82	9487.26	12.11
Total	80615.7	100.00	79800.7	100.00	-815.04	0

The 60.1-80% class has decreased by 11892.8 ha (14.25%). As evident from the table 11 and Map 8, this decrease is due to the fact that a large portion of the class i.e., 15092.73 ha has been restocked from 1989 to 2003, thus has converted from 60.1-80 to 80.1-100 class which is in-fact a desirable change. Also, from Table 11, it is evident that the increase in 80.1-100% class from 1989 to 2003 is largely due to the increase in FCC in the 60.1-80% class because about 99% of the increase in 80.1-100% class is due to restocking of 60.1-80% class. The spatial distribution of the trade-off between 60.1-80 and 80.1-100 class is given in Map 8.

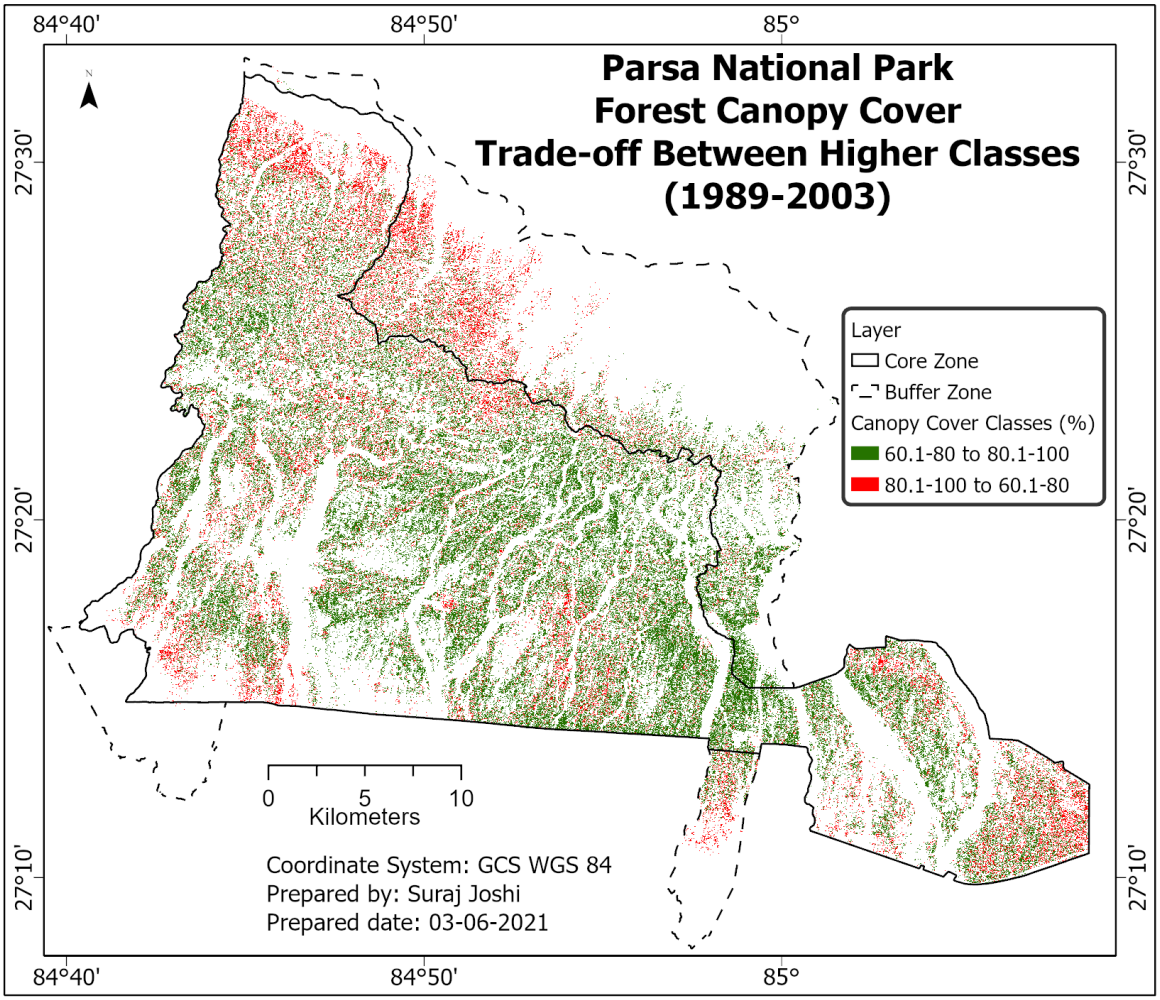

Map 8: Parsa national park canopy cover trade-off between higher classes (1989-2003)

Table 11: Canopy cover change matrix (1989-2003)

1989 (Along Rows)	2003 (Along Columns)					
	FCC Classes	0-20	20.1-40	40.1-60	60.1-80	80.1-100
	0-20	230.04	274.41	135.63	35.1	0.54
	20.1-40	361.8	776.97	692.91	184.68	7.92
	40.1-60	288.27	1097.73	3196.08	2539.35	117.72
	60.1-80	106.11	502.11	4137.48	31014.81	15092.73
	80.1-100	8.19	29.97	194.31	5487.39	11764.17

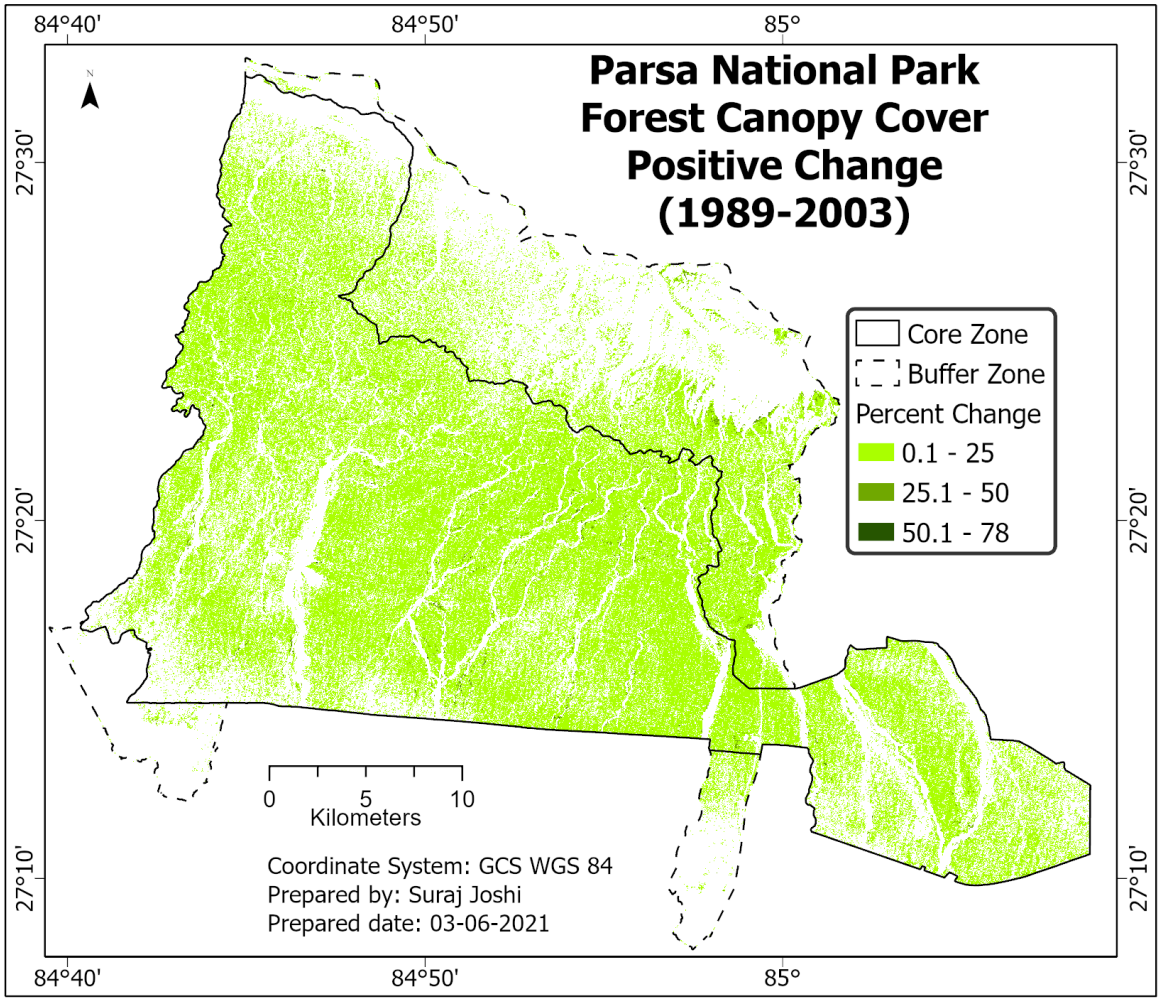

Map 9: Parsa national park canopy cover positive change (1989-2003)

FCC in most of the forest area from 1989 to 2003 was found to have increased by 0.1-25%. FCC decrease by 0.1-25% can mostly be seen in the forest inside the buffer zone or near it. The decrease in FCC above 25% can be clearly seen in some parts of the buffer zone. On the hand, FCC increase above 25% is negligible. The overall FCC change from

1989 to 2003 is given in the Map 7, and positive and negative FCC change is given in Map 9 and Map 10 respectively.

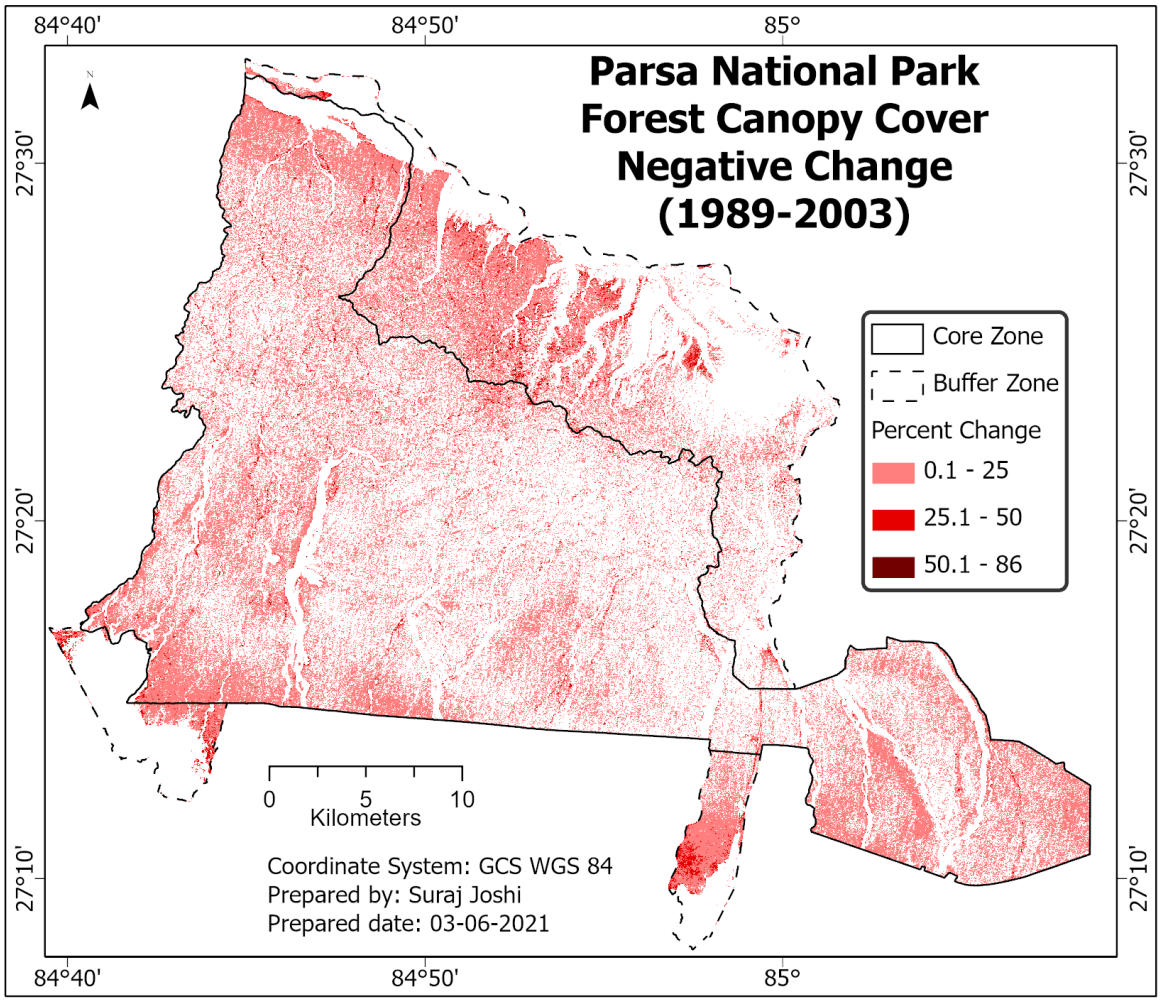

Map 10: Parsa national park canopy cover negative change (1989-2003)

3.2.2. FCC Change (2003-2019)

In contrast to FCC change from 1989 to 2003, area of the FCC classes has not changed drastically from 2003 to 2019. Except for 40.1-60% class, the changes in all the other classes were below 1%. The 0-20%, 20.1-40% classes have decreased by 0.15% and 0.14% respectively. On the other hand, 60.1-80% and 80.1-100% classes have increased by 0.84% and 0.59% respectively. The change in different FCC classes from 2003 to 2019 is given in Table 12 and its spatial distribution is given in Map 11.

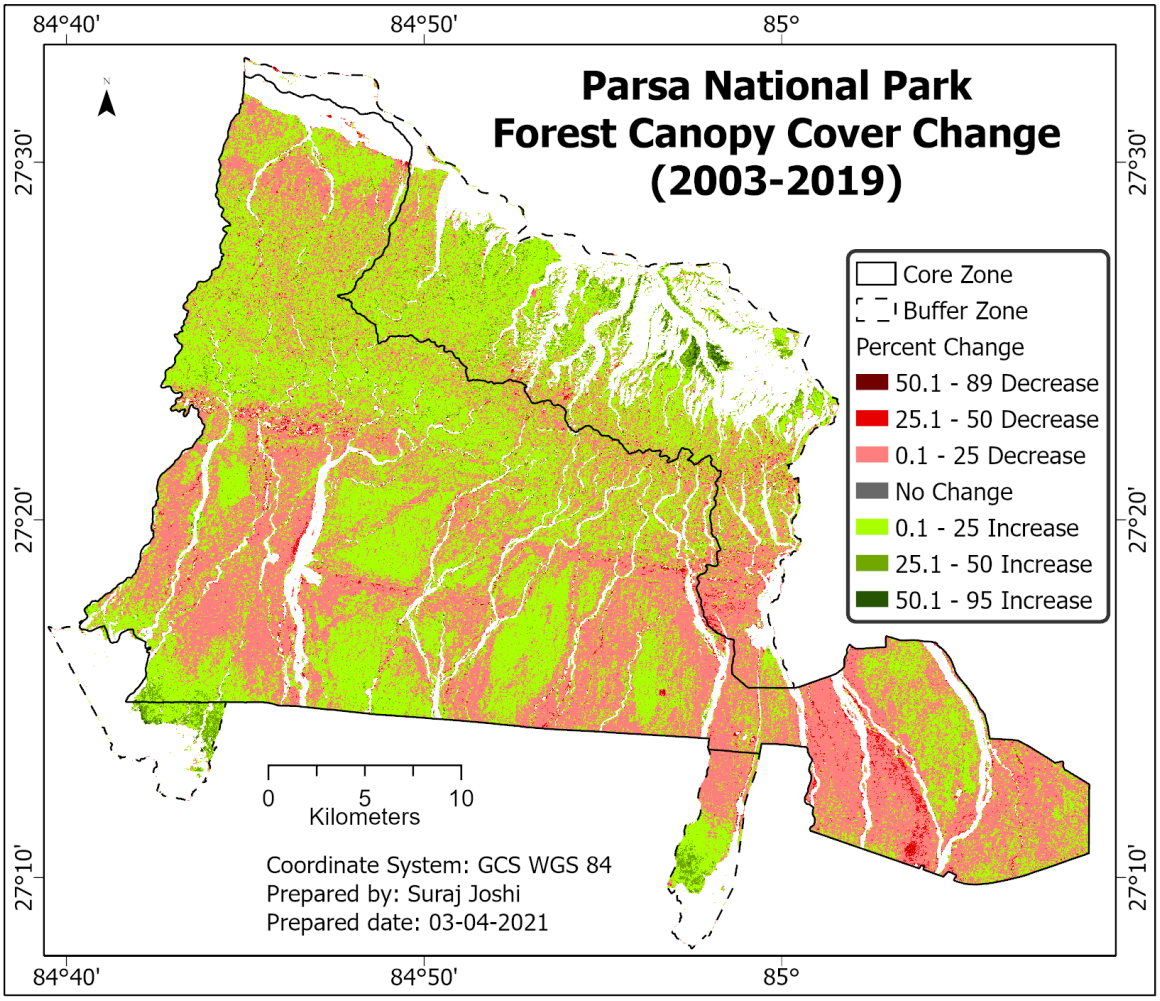

Map 11: Parsa national park canopy cover change (2003-2019)

Table 12: Canopy cover change (2003-2019)

	2003		2019		Change (2003-2019)	
Classes	Area (ha)	Area (%)	Area (ha)	Area (%)	Area (ha)	Area (%)
0-20	1539.0	1.93	1440.1	1.78	-98.9	-0.15
20.1-40	3275.3	4.10	3200.7	3.96	-74.6	-0.14
40.1-60	8669.8	10.86	7861.2	9.73	-808.6	-1.14
60.1-80	39331.5	49.29	40510.1	50.13	1178.6	0.84
80.1-100	26985.1	33.82	27805.7	34.41	820.6	0.59
Total	79800.7	100.00	80817.8	100.00	1017.1	0.00

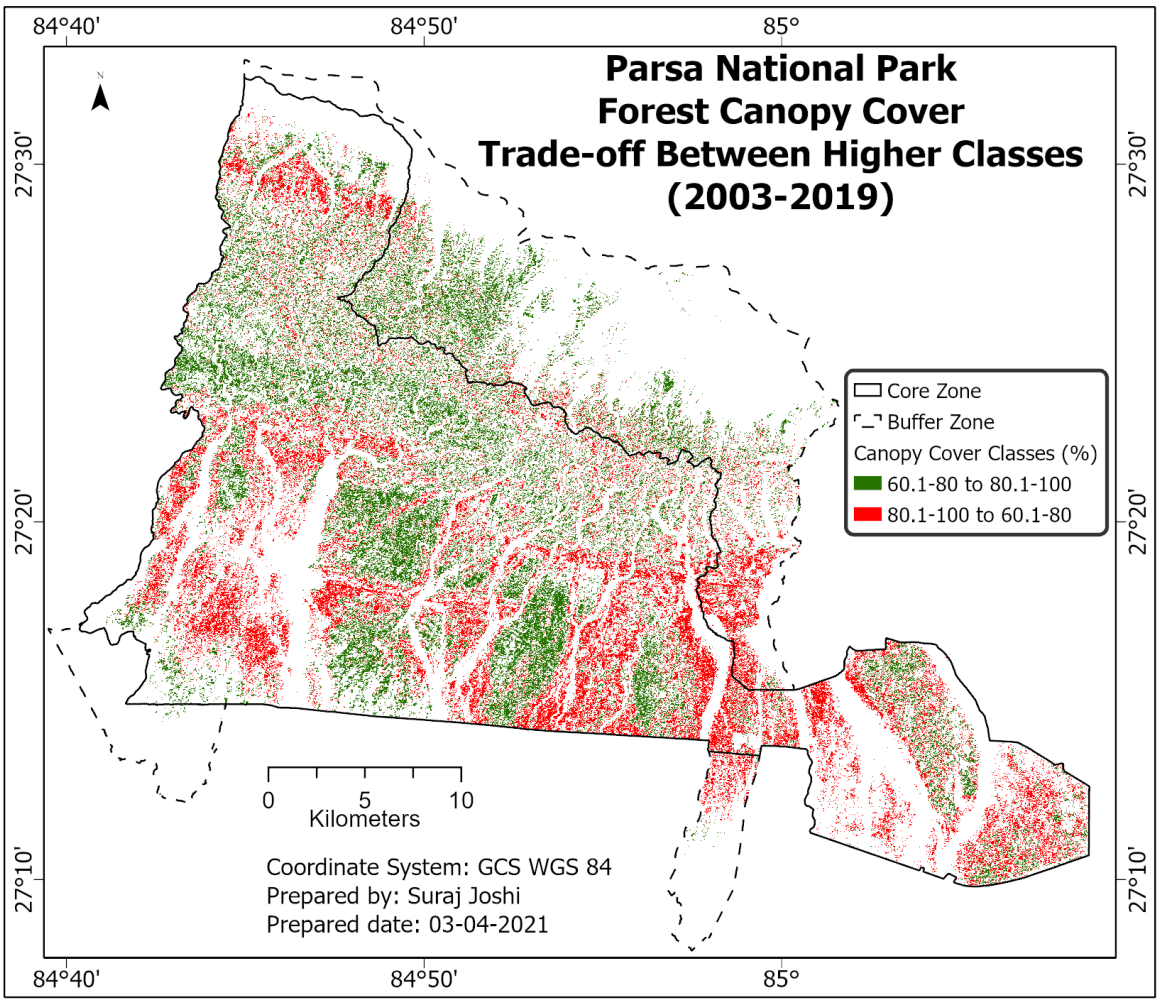

Map 12: Parsa national park canopy cover trade-off between higher classes(2003-2019)

Similar to the changes that occurred from 1989 to 2003, a trade-off relationship can be observed between the 60.1-80 and 80.1-100 class (see Table 13). Table 13 shows that about 11000 ha area of 60.1-80% class has seen an increase in FCC thus turning in 80.1-100% class, while same area of 80.1-100% class has decreased in FCC and changed into 60.1-80% class. The spatial distribution of this trade-off can be observed in Map 12.

FCC in most of the forest area from 2003 to 2019 was found to be either increased or decreased by 0.1-25%. Most parts of the buffer zone forest have increased in FCC, whereas FCC decrease can mostly be seen in the forest areas with flat terrain. The decrease in FCC above 25% is negligible but can be clearly seen in the extended part of the park. Also, some parts of the buffer zone forest have increased in FCC by more than

25% and even by more than 50%. The FCC change from 2003 to 2019 is given in the Map 12 and the positive and negative change is given in Map 13 and Map 14 respectively.

Table 13: Canopy cover change matrix (2003-2019)

2003 (Along Rows)	2019 (Along Columns)					
	FCC Classes	0-20	20.1-40	40.1-60	60.1-80	80.1-100
	0-20	176.94	342.18	371.25	220.23	14.76
	20.1-40	255.96	632.61	991.26	843.75	65.88
	40.1-60	239.49	887.85	2336.49	4267.98	542.16
	60.1-80	68.49	325.53	3190.86	23999.13	11524.68
	80.1-100	8.55	36.45	291.15	10984.59	15646.95

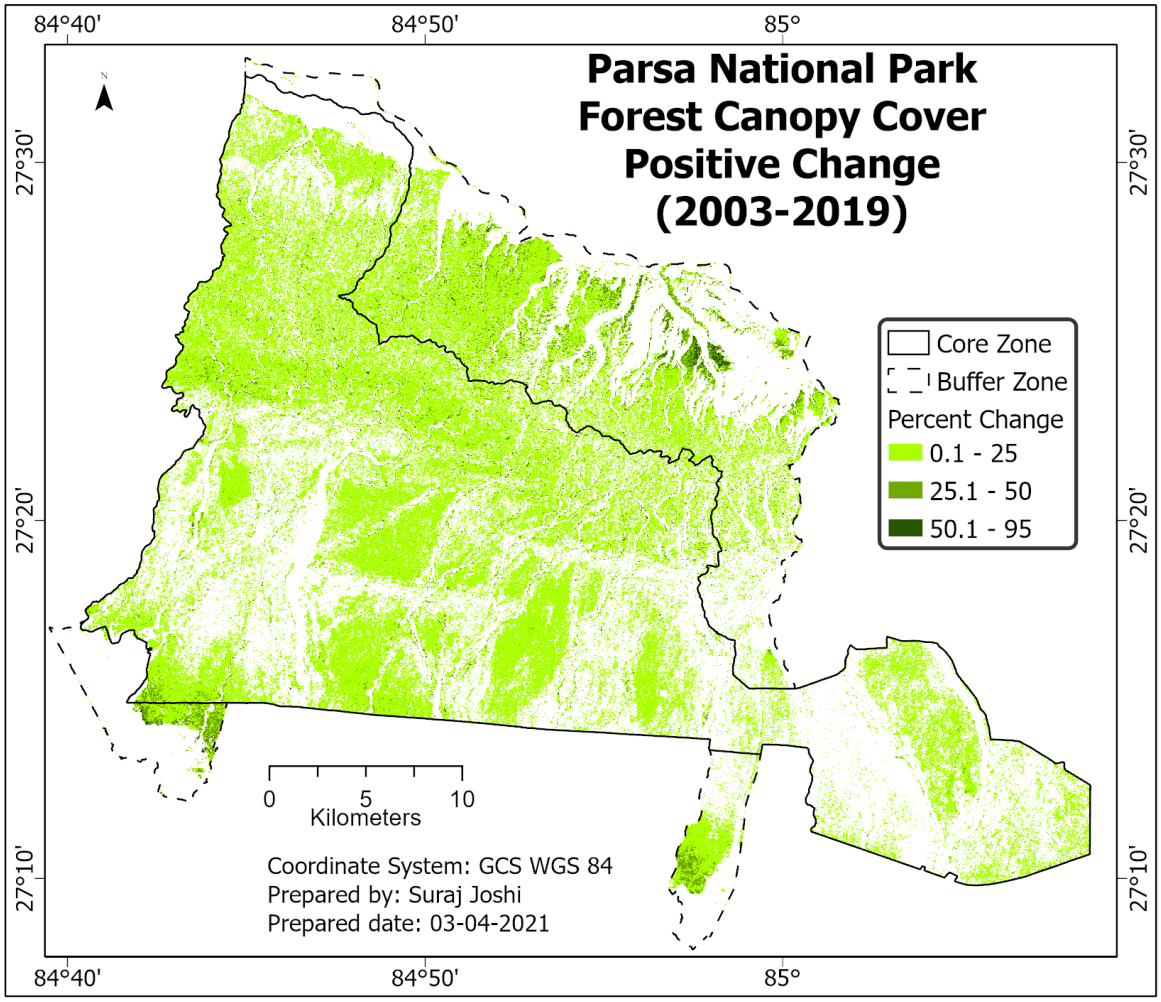

Map 13: Parsa national park canopy cover positive change (2003-2019)

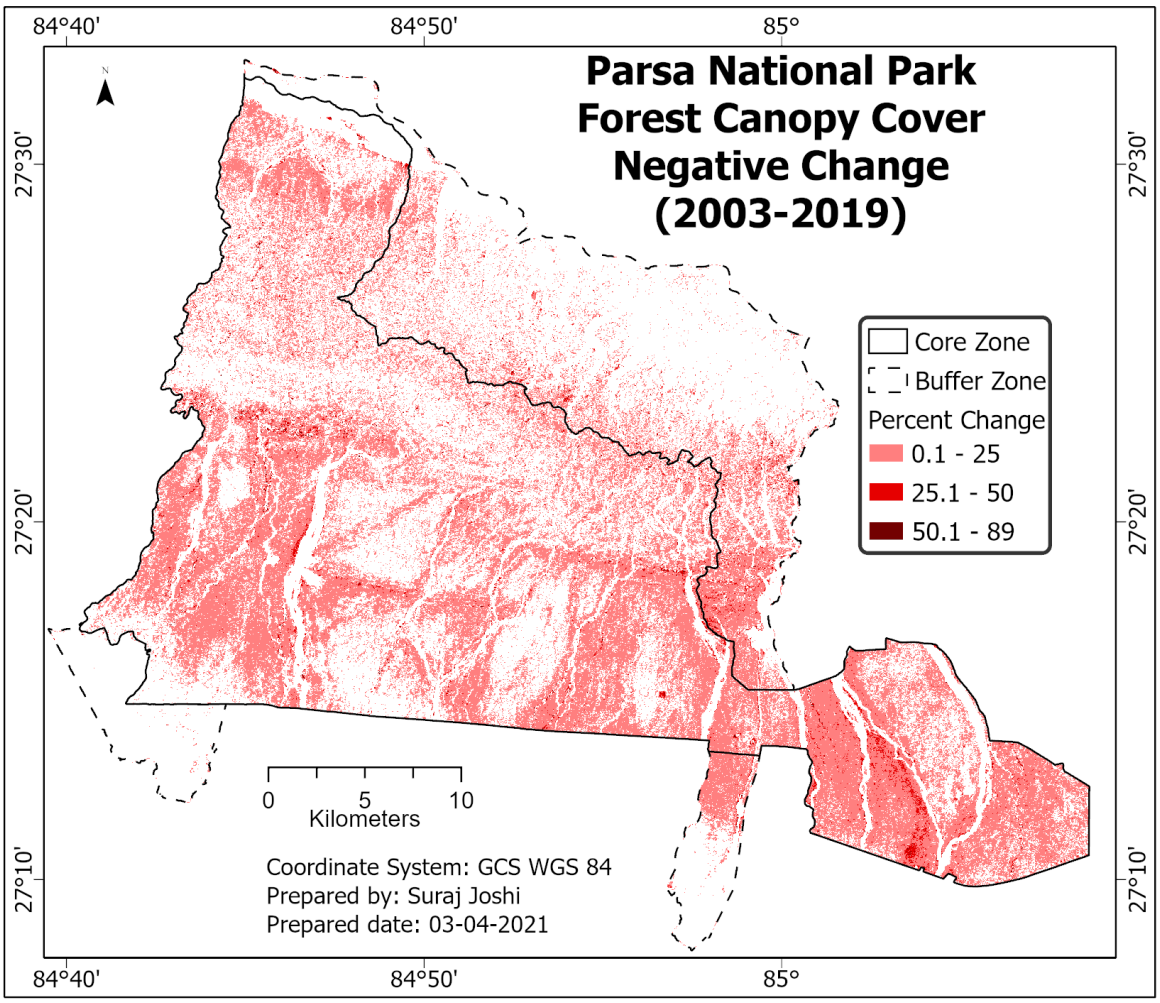

Map 14: Parsa national park canopy cover negative change (2003-2019)

Chapter-4: Conclusion

This study assessed the long-term FCC change in Parsa national park, Nepal from 1989 to 2019. FCC change in the park was studied within time periods of 1989-2003 and 2003-2019 using FCD model. The result shows that, even though the forest in terms of area has not changed much in the study period, FCC in the forest was found to be dynamic. In both time periods, mostly the forest areas with higher FCC i.e., 60.1-100% have changed significantly as compared to areas with lower FCC.

In general, a positive trend of FCC change was observed in the core zone, whereas FFC change in the buffer zone was mostly negative from 1989 to 2003 and positive from 2003 to 2019. Despite of that, forest in the northeastern part of the buffer zone had positive change in both the time periods indicating a positive trend. In terms of intensity/degree of FCC change i.e., percentage increase/decrease in FCC, both increase and decrease were mostly in the range of 0.1% to 25%. FCC in some parts of the buffer zone was found to be increased by more than 25%, and even by more than 50% from 2003 to 2019. In contrast to that, in the same period, FCC in some parts of the extended park area to the south-east was found to be decreased by more than 25%. A negative trend was observed for the same parts of the extended area.

This study helped to understand the dynamics of forest cover change in Parsa national park, not only in terms of area, but also the spatio-temporal change in the forest canopy cover. This will help the park authorities in planning effective management strategies to ensure conservation of the forest resources and long-term benefits to the local people. In general, FCC in majority of the core area shows an increasing trend. In contrast to that, no clear trend i.e., no increasing or decreasing trend was observed in majority of the buffer zone forests. Thus, management interventions might be needed in buffer zone to ensure that the forests are properly managed, and the growth of the forest is optimum. A

continuous periodic monitoring of the forest using satellite imagery is also recommended to study forest cover change in the future. Beside monitoring the forest cover change, it important to understand the probable reasons that might have caused the change in FCC over the study period to devise effective management strategies. Thus, it is recommended that further studies be carried out to understand the factors causing FCC change in the park.

References

Abdi, H., & Williams, L. J. (2010). Principal component analysis. *WIREs Computational Statistics*, *2*(4), 433–459. https://doi.org/10.1002/wics.101 (Accessed date: 19-05-2021)

Bruce, C. M., & Hilbert, D. W. (2006). *Pre-processing methodology for application to Landsat TM/ETM+ imagery of the wet tropics*. Cooperative Research Centre for Tropical Rainforest Ecology and Management. http://rainforest-crc.jcu.edu.au/publications/landsat_preprocessing.pdf (Accessed date: 28-09-2020)

Carreiras, J. M. B., Pereira, J. M. C., & Pereira, J. S. (2006). Estimation of tree canopy cover in evergreen oak woodlands using remote sensing. *Forest Ecology and Management*, *223*(1), 45–53. https://doi.org/10.1016/j.foreco.2005.10.056 (Accessed date: 19-05-2021) (Accessed date: 23-04-2021)

Chaudhary, R. P., Uprety, Y., & Rimal, S. K. (2016). Deforestation in Nepal. In *Biological and Environmental Hazards, Risks, and Disasters* (pp. 335–372). Elsevier. https://doi.org/10.1016/B978-0-12-394847-2.00020-6 (Accessed date: 23-04-2021)

DFRS. (2014). *Terai forests of Nepal* (Resource Assessment Nepal Project). Department of Forest Research and Survey, Ministry of Forests and Soil Conservation, Government of Nepal. http://frtc.gov.np/downloadfile/The-TeraiForestsofNepal_1579845265.pdf (Accessed date: 28-01-2021)

DFRS. (2015). *State of Nepal's forests* (Forest Resource Assessment Nepal). Department of Forest Research and Survey. (Accessed date: 28-01-2021)

Dymond, J. R., & Shepherd, J. D. (1999). Correction of the topographic effect in remote sensing. *IEEE Transactions on Geoscience and Remote Sensing*, *37*(5), 2618–2619. https://doi.org/10.1109/36.789656 (Accessed date: 08-04-2021)

Echeverría, C., Newton, A. C., Lara, A., Benayas, J. M. R., & Coomes, D. A. (2007). Impacts of forest fragmentation on species composition and forest structure in the temperate landscape of southern Chile. *Global Ecology and Biogeography*, *16*(4), 426–439. https://doi.org/10.1111/j.1466-8238.2007.00311.x (Accessed date: 28-01-2021)

Esri. (2021a). *How Rescale by Function works—ArcGIS Pro | Documentation*. https://pro.arcgis.com/en/pro-app/latest/tool-reference/spatial-analyst/how-rescale-by-function-works.htm (Accessed date: 11-04-2021)

Esri. (2021b). *The transformation functions available for Rescale by Function—ArcGIS Pro | Documentation*. https://pro.arcgis.com/en/pro-app/latest/tool-reference/spatial-analyst/the-transformation-functions-available-for-rescale-by-function.htm (Accessed date: 11-04-2021)

FAO. (1995). Chapter 3 Why are forests important? In *The Challenge of Sustainable Forest Management: What future for the world's forests?* FAO. http://www.fao.org/3/t0829e/T0829E05.htm#Chapter%203%20Why%20are%20forests%20important (Accessed date: 10-11-2020)

Frazer, G. W., Fournier, R. A., Trofymow, J. A., & Hall, R. J. (2001). A comparison of digital and film fisheye photography for analysis of forest canopy structure and gap light transmission. *Agricultural and Forest Meteorology*, *109*(4), 249–263. https://doi.org/10.1016/S0168-1923(01)00274-X (Accessed date: 06-05-2021)

Gitelson, A. A. (2004). Wide Dynamic Range Vegetation Index for Remote Quantification of Biophysical Characteristics of Vegetation. *Journal of Plant Physiology*, *161*(2), 165–173. https://doi.org/10.1078/0176-1617-01176 (Accessed date: 11-04-2021)

Godinho, S., Gil, A., Guiomar, N., Neves, N., & Pinto-Correia, T. (2014). A remote sensing-based approach to estimating montado canopy density using the FCD model: A contribution to identifying HNV farmlands in southern Portugal. *Agroforestry Systems*, *90*(1), 23–34. https://doi.org/10.1007/s10457-014-9769-3 (Accessed date: 25-04-2021)

Google Earth Engine. (n.d.-a). *USGS Landsat 5 Surface Reflectance Tier 1*. Earth Engine Data Catalog. Retrieved August 28, 2020, from https://developers.google.com/earth-engine/datasets/catalog/LANDSAT_LT05_C01_T1_SR

Google Earth Engine. (n.d.-b). *USGS Landsat 8 Surface Reflectance Tier 1*. Earth Engine Data Catalog. Retrieved August 28, 2020, from https://developers.google.com/earth-engine/datasets/catalog/LANDSAT_LC08_C01_T1_SR

Gorelick, N., Hancher, M., Dixon, M., Ilyushchenko, S., Thau, D., & Moore, R. (2017). Google Earth Engine: Planetary-scale geospatial analysis for everyone. *Remote Sensing of Environment*, *202*, 18–27. https://doi.org/10.1016/j.rse.2017.06.031 (Accessed date: 28-10-2020)

Hansen, M. C., Potapov, P. V., Moore, R., Hancher, M., Turubanova, S. A., Tyukavina, A., Thau, D., Stehman, S. V., Goetz, S. J., Loveland, T. R., Kommareddy, A., Egorov, A., Chini, L., Justice, C. O., & Townshend, J. R. G. (2013). High-Resolution Global Maps of 21st-Century Forest Cover Change. *Science*, *342*(6160), 850–853. https://doi.org/10.1126/science.1244693 (Accessed date: 28-10-2020)

Henning, J. G., & Radtke, P. J. (2006). Ground-based Laser Imaging for Assessing Three-dimensional Forest Canopy Structure. *Photogrammetric Engineering & Remote Sensing*, *72*(12), 1349–1358. https://doi.org/10.14358/PERS.72.12.1349 (Accessed date: 06-05-2021)

Hurni, K., Heinimann, A., & Würsch, L. (2017). *Google Earth Engine Image Pre-processing Tool: Background and Methods*. https://www.cde.unibe.ch/e65013/e542846/e707304/e707386/e707388/CDE_Pre-processingTool-BackgroundAndMethods_eng.pdf (Accessed date: 08-04-2021)

ITTO & JOFCA. (1999). *FCD-Mapper User's Guide*. http://www.itto.int/files/itto_project_db_input/2056/Technical/pd13-97-3%20rev1(F)%20FCD-Mapper%20User%27s%20Guide_e.pdf (Accessed date: 10-04-2021)

Jain, P., Ahmed, R., Rehman, S., & Sajjad, H. (2020). Detecting disturbed forest tracts in the Sariska Tiger Reserve, India, using forest canopy density and fragmentation models. *Modeling Earth Systems and Environment*, *6*(3), 1373–1385.

https://doi.org/10.1007/s40808-020-00755-4 (Accessed date: 28-01-2021)

Jennings, S. (1999). Assessing forest canopies and understorey illumination: Canopy closure, canopy cover and other measures. *Forestry*, *72*(1), 59–74. https://doi.org/10.1093/forestry/72.1.59 (Accessed date: 19-02-2021)

Jiang, Z., Huete, A. R., Chen, J., Chen, Y., Li, J., Yan, G., & Zhang, X. (2006). Analysis of NDVI and scaled difference vegetation index retrievals of vegetation fraction. *Remote Sensing of Environment*, *101*(3), 366–378. https://doi.org/10.1016/j.rse.2006.01.003 (Accessed date: 11-04-2021)

Joshi, C., Leeuw, J. D., Skidmore, A. K., Duren, I. C. van, & van Oosten, H. (2006). Remotely sensed estimation of forest canopy density: A comparison of the performance of four methods. *International Journal of Applied Earth Observation and Geoinformation*, *8*(2), 84–95. https://doi.org/10.1016/j.jag.2005.08.004 (Accessed date: 10-02-2021)

Korhonen, L., Korhonen, K. T., Rautiainen, M., & Stenberg, P. (2006). Estimation of forest canopy cover: A comparison of field measurement techniques. *Silva Fennica*, *40*(4), 577–588. https://doi.org/10.14214/sf.315 (Accessed date: 22-04-2021)

Lambin, E. F., Geist, H. J., & Lepers, E. (2003). Dynamics of Land-Use and Land-Cover Change in Tropical Regions. *Annual Review of Environment and Resources*, *28*(1), 205–241. https://doi.org/10.1146/annurev.energy.28.050302.105459 (Accessed date: 28-01-2021)

Lu, D., & Weng, Q. (2007). A survey of image classification methods and techniques for improving classification performance. *International Journal of Remote Sensing*, *28*(5), 823–870. https://doi.org/10.1080/01431160600746456 (Accessed date: 01-09-2020)

Ma, Q., Su, Y., & Guo, Q. (2017). Comparison of Canopy Cover Estimations From Airborne LiDAR, Aerial Imagery, and Satellite Imagery. *IEEE Journal of Selected Topics in Applied Earth Observations and Remote Sensing*, *10*(9), 4225–4236. https://doi.org/10.1109/JSTARS.2017.2711482 (Accessed date: 27-04-2021)

Millard, K., & Richardson, M. (2015). On the Importance of Training Data Sample Selection in Random Forest Image Classification: A Case Study in Peatland Ecosystem Mapping. *Remote Sensing*, *7*(7), 8489–8515. https://doi.org/10.3390/rs70708489 (Accessed date: 01-09-2020)

Nagendra, H. (2002). Tenure and forest conditions: Community forestry in the Nepal Terai. *Environmental Conservation*, *29*, 530–539. https://doi.org/10.1017/S0376892902000383 (Accessed date: 21-01-2021)

Paletto, A., & Tosi, V. (2009). Forest canopy cover and canopy closure: Comparison of assessment techniques. *European Journal of Forest Research*, *128*, 265–272. https://doi.org/10.1007/s10342-009-0262-x (Accessed date: 14-02-2021)

Panta, M., Kim, K., & Joshi, C. (2008). Temporal mapping of deforestation and forest degradation in Nepal: Applications to forest conservation. *Forest Ecology and Management*, *256*(9), 1587–1595. https://doi.org/10.1016/j.foreco.2008.07.023 (Accessed date: 26-04-2021)

Parsa National Park. (2018). *Parsa National Park and its Buffer Zone Management Plan, FY 2075/76-2079/80*. Parsa National Park Office. http://dnpwc.gov.np/media/publication/Parsa_National_Park__Management_Plan_2075.pdf (Accessed date: 25-08-2020)

Pathak, B. R., Xie, Y., & Bohara, R. (2017). Community Based Forestry in Nepal: Status, Issues and Lessons Learned. *International Journal of Sciences*, *6*, 119–129. https://doi.org/10.18483/ijSci.1232 (Accessed date: 26-05-2021)

Pimple, U., Sitthi, A., Simonetti, D., Pungkul, S., Leadprathom, K., & Chidthaisong, A. (2017). Topographic Correction of Landsat TM-5 and Landsat OLI-8 Imagery to Improve the Performance of Forest Classification in the Mountainous Terrain of Northeast Thailand. *Sustainability*, *9*(2), 258. https://doi.org/10.3390/su9020258 (Accessed date: 26-04-2021)

Purevdorj, T., Tateishi, R., Ishiyama, T., & Honda, Y. (1998). Relationships between percent vegetation cover and vegetation indices. *International Journal of Remote Sensing*, *19*(18), 3519–3535. https://doi.org/10.1080/014311698213795 (Accessed date: 11-04-2021)

Reddy, S., Vazeed Pasha, S., Satish, K. V., Saranya, K. R. L., Jha, C. S., & Krishna Murthy, Y. V. N. (2018). Quantifying nationwide land cover and historical changes in forests of Nepal (1930–2014): Implications on forest fragmentation. *Biodiversity and Conservation*, *27*(1), 91–107. https://doi.org/10.1007/s10531-017-1423-8 (Accessed date: 28-01-2021)

Richards, J. A. (2013). *Remote Sensing Digital Image Analysis* (5th ed.). Springer Berlin Heidelberg. https://doi.org/10.1007/978-3-642-30062-2 (Accessed date: 18-05-2021)

Rikimaru, A. (1996). *Landsat TM Data processing guide for forest canopy density mapping and monitoring model* (PO 32/93 Rev.2 (F); Utilization of Remote Sensing in Site Assessment and Planning for Rehabilitation of Logged-over Forests, pp. 1–8). ITTO. https://www.itto.int/files/itto_project_db_input/2205/Technical/pd32-93%20rev2(F)%20e_Utilization%20of%20Remote%20Sensing%20in%20Site%20Assessment%20and%20Planning_E.pdf (Accessed date: 07-10-2020)

Rikimaru, A., Roy, P. S., & Miyatake, S. (2002). Tropical forest cover density mapping. *Tropical Ecology*, *43*(1), 39–47. /paper/Tropical-forest-cover-https://tropecol.com/pdf/open/PDF_43_1/43104.pdf (Accessed date: 07-10-2020)

Rodarmel, C., & Shan, J. (2002). Principal Component Analysis for Hyperspectral Image Classification. *Surveying and Land Information Systems*, *62*(2), 115. (Accessed date: 19-05-2021)

Rodriguez-Galiano, V. F., Chica-Olmo, M., Abarca-Hernandez, F., Atkinson, P. M., & Jeganathan, C. (2012). Random Forest classification of Mediterranean land cover using multi-seasonal imagery and multi-seasonal texture. *Remote Sensing of Environment*, *121*, 93–107. https://doi.org/10.1016/j.rse.2011.12.003 (Accessed date: 13-09-2020)

Rodriguez-Galiano, V. F., Ghimire, B., Rogan, J., Chica-Olmo, M., & Rigol-Sanchez, J. P. (2012). An assessment of the effectiveness of a random forest classifier for land-cover classification. *ISPRS Journal of Photogrammetry and Remote Sensing*, *67*,

93–104. https://doi.org/10.1016/j.isprsjprs.2011.11.002 (Accessed date: 13-09-2020)

Sahana, M., Sajjad, H., & Ahmed, R. (2015). Assessing spatio-temporal health of forest cover using forest canopy density model and forest fragmentation approach in Sundarban reserve forest, India. *Modeling Earth Systems and Environment*, *1*(4), 49. https://doi.org/10.1007/s40808-015-0043-0 (Accessed date: 28-01-2021)

Tupin, F., Inglada, J., & Nicolas, J.-M. (2014). *Remote Sensing Imagery*. John Wiley & Sons.

USGS. (n.d.). *Landsat Levels of Processing*. USGS. Retrieved August 28, 2020, from https://www.usgs.gov/land-resources/nli/landsat/landsat-levels-processing

USGS. (2019). *Landsat 8 (L8) Data Users Handbook*. https://prd-wret.s3.us-west-2.amazonaws.com/assets/palladium/production/atoms/files/LSDS-1574_L8_Data_Users_Handbook-v5.0.pdf (Accessed date: 25-12-2020)

USGS. (2020a). *Landsat 4-7 Collection 1 (C1) Surface Reflectance (LEDAPS) Product Guide*. USGS. https://prd-wret.s3.us-west-2.amazonaws.com/assets/palladium/production/atoms/files/LSDS-1370_L4-7_C1-SurfaceReflectance-LEDAPS_ProductGuide-v3.pdf (Accessed date: 25-10-2020)

USGS. (2020b). *Landsat 8 Collection 1 (C1) Land Surface Reflectance Code (LaSRC) Product Guide*. USGS. https://prd-wret.s3.us-west-2.amazonaws.com/assets/palladium/production/atoms/files/LSDS-1368_L8_C1-LandSurfaceReflectanceCode-LASRC_ProductGuide-v3.pdf (Accessed date: 25-10-2020)

Xue, J., & Su, B. (2017, May 23). *Significant Remote Sensing Vegetation Indices: A Review of Developments and Applications* [Review Article]. Journal of Sensors; Hindawi. https://doi.org/10.1155/2017/1353691 (Accessed date: 29-06-2020)

Yan, G., Mas, J.-F., Maathuis, B. H. P., Xiangmin, Z., & Dijk, P. M. V. (2007). Comparison of pixel-based and object-oriented image classification approaches—A case study in a coal fire area, Wuda, Inner Mongolia, China. *International Journal of Remote Sensing*, *27*(18). https://doi.org/10.1080/01431160600702632 (Accessed date: 13-09-2020)

Young, N. E., Anderson, R. S., Chignell, S. M., Vorster, A. G., Lawrence, R., & Evangelista, P. H. (2017). A survival guide to Landsat preprocessing. *Ecology*, *98*(4), 920–932. https://doi.org/10.1002/ecy.1730 (Accessed date: 25-10-2020)

Appendix: Parsa National Park Land Cover Status in 1989, 2003 and 2019

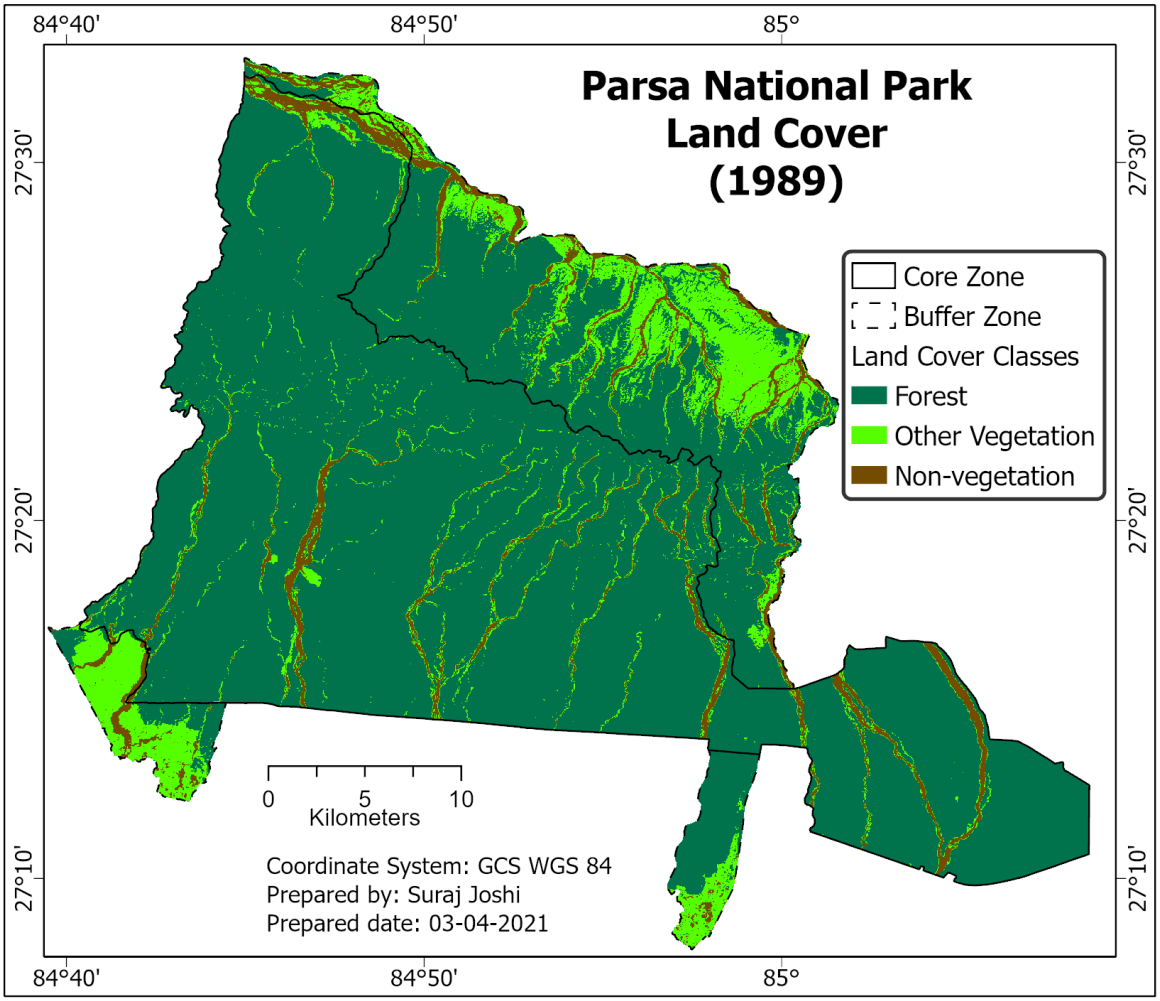

Map 15: Parsa national park land cover (1989)

Table 14: Accuracy assessment (1989)

		Test Samples				
		Forest	Other Vegetation	Non-vegetation	Total	User`s Accuracy
Classified Image	Forest	42	0	0	42	95%
	Other Vegetation	2	40	0	42	100%
	Non-Vegetation	0	0	42	42	100%
Total		44	40	42	Overall Accuracy= 98%	
Producer`s Accuracy		100%	95%	100%	Kappa Coefficient=0.97	

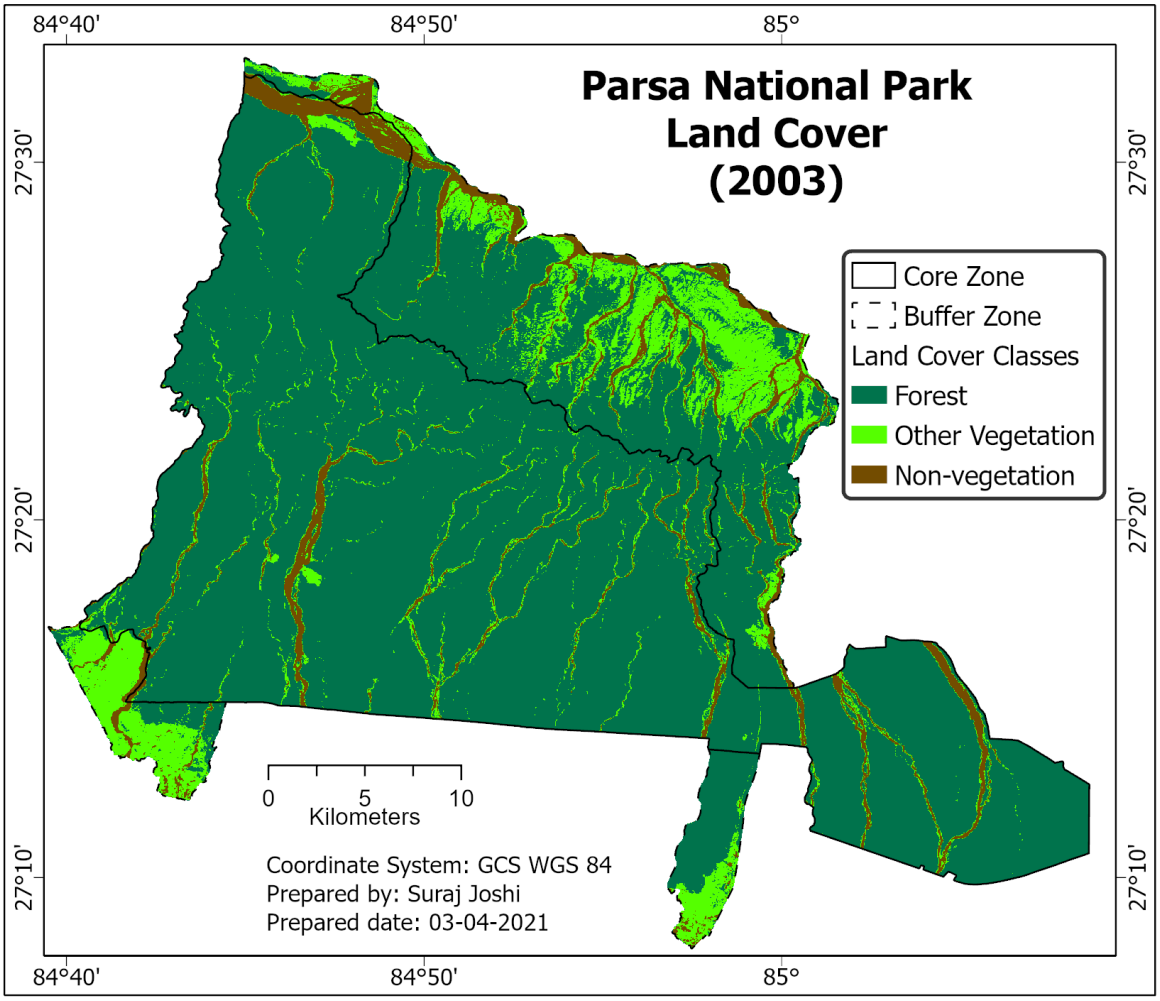

Map 16: Parsa national park land cover (2003)

Table 15: Accuracy assessment (2003)

		Test Samples				
		Forest	Other Vegetation	Non-vegetation	Total	User`s Accuracy
Classified Image	Forest	42	0	0	42	95%
	Other Vegetation	1	39	2	42	100%
	Non-Vegetation	1	0	41	42	100%
Total		44	39	43	Overall Accuracy= 96.8%	
Producer`s Accuracy		100%	95%	100%	Kappa Coefficient=0.95	

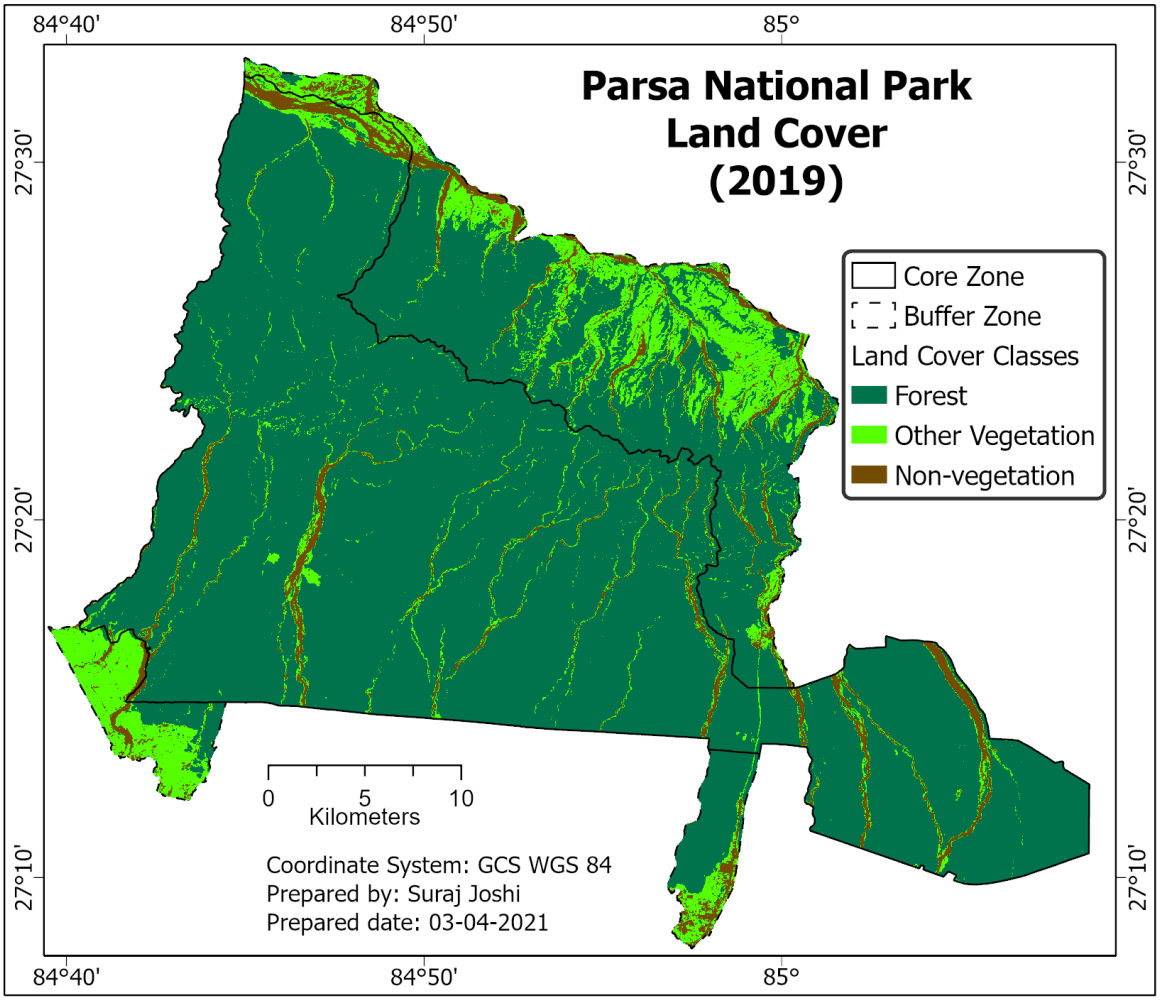

Map 17: Parsa national park land cover (2019)

Table 16: Accuracy Assessment (2019)

		Test Samples				
		Forest	Other Vegetation	Non-vegetation	Total	User`s Accuracy
Classified Image	Forest	42	0	0	42	100%
	Other Vegetation	0	38	4	42	90.4%
	Non-Vegetation	0	0	42	42	100%
Total		42	38	46	Overall Accuracy= 96.8%	
Producer`s Accuracy		100%	100%	91.3%	Kappa Coefficient=0.95	

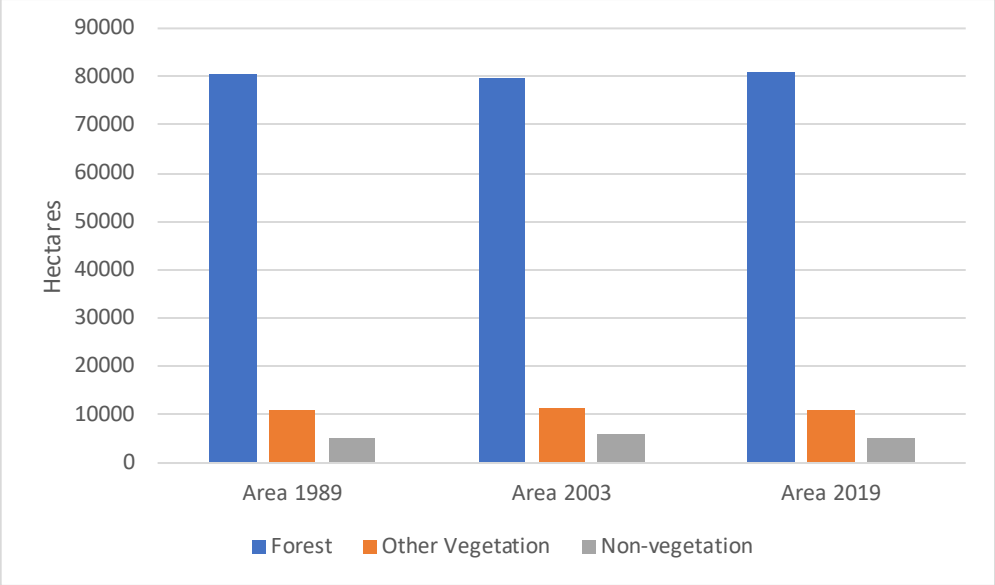

Figure 25: Parsa national park land cover status in 1989, 2003 and 2019